Conceptual design of a dual reactive dividing wall column for downstream processing of lactic acid

DOI:
10.1016/j.cep.2021.108402

Document Version
Accepted author manuscript

Conceptual design of a dual reactive dividing wall column for downstream processing of lactic acid

Isabel Pazmiño-Mayorga, Megan Jobson, Anton A. Kiss

Department of Chemical Engineering and Analytical Science, The University of Manchester, Sackville Street, Manchester, M13 9PL, United Kingdom

Keywords

Process intensification; process design and simulation; process synthesis; reactive distillation

Highlights

- Novel dual reactive dividing wall column for processing bio-based lactic acid
- Methodology for synthesis and design of a dual reactive distillation column
- Advanced reactive distillation overcomes challenging separations (reactive impurities)

Abstract

Methodologies for designing intensified processing units are necessary to enable the industrial application of process intensification concepts. This article presents a ruled-based systematic methodology for the synthesis and conceptual design of a dual reactive dividing wall column (dual R-DWC). A decomposition approach is used to identify the tasks required for the separation by introducing a reactive separating agent to exploit a reversible reaction to enhance the driving forces. A combination of shortcut and rigorous simulations led to the conceptual design of a novel dual R-DWC in which the forward and reverse reactions and the separation occur at once.

The methodology was demonstrated in a case study for the separation of lactic acid from dilute aqueous streams and a reactive impurity that hinder the lactic acid conversion and its recovery, while the byproducts may bring new challenges for the desired separations.

This study is the first to investigate the effect of reactive impurities on the reaction and the separation, hence adding a more realistic framework to the design. The flowsheet produced was evaluated against benchmark processes and showed a significant process improvement in terms of energy savings (ranging 13-27 %), material intensity (28-32 % reduction), and water consumption (22-36 % reduction), while the reactive impurities are effectively removed.

1. Introduction

The chemical industry faces increasing competitiveness and environmental regulatory constraints, which demand new approaches to improve different supply chain stages, process performance and operation mode. For example, the introduction of process intensification (PI) has been reported for various technologies and products bringing significant benefits to the process without constraints limited to the unit-operation classical concept (Gorak and Stankiewicz, 2018). The application of PI to the design of chemical processes has demonstrated significant improvements in terms of efficiency, economics, safety and environmental performance due to the reduction of equipment size, energy consumption and waste formation (Moulijn and Stanckiewicz, 2017). One approach to incorporate PI in the design of chemical processes is combining functions leading to a synergistic effect that shows better process performance than the separate functions, i.e., reactive distillation (Stankiewicz et al., 2019). Reactive distillation (RD) exploits the synergy of the combined reaction and separation, which leads to benefits, such as separation improvement as the reaction overcomes azeotropes, and reaction improvement as the separation overcomes chemical equilibrium and enhances reaction rates, conversion and selectivity due to the constant removal of the reaction products (Kiss, 2017). Additional benefits arise when comparing the performance of RD with the conventional reactor-distillation sequence, such as capital and operating costs savings, less plant footprint, less recycling streams, and better environmental performance (Sundmacher and Kienle, 2003). Nevertheless, some constraints to RD's application need to be overcome. For example, specific ranges of temperatures and pressures must overlap, in addition to the limitations due to the thermal stability and the catalyst's life span (Orjuela et al., 2016).

Novel RD configurations with additional process intensification features (advanced reactive distillation technologies: R-DWC, R-HiGee, CCD, R-HIDiC, MA-RD) have attracted academic and industrial attention due to their potential to expand the applicability of RD. A survey, based on industrial and academic experience, qualitatively shows the degree of development of several advanced reactive distillation technologies in different aspects, including availability of methods and tools for design, simulation, dynamics and control as well as practical challenges (Kiss et al., 2019). Among them, the R-DWC presents greater development and ease of implementation, as extended benefits of the dividing wall column (DWC) applied for reactive systems, as described in a recent review paper about R-DWC (Weinfeld et al., 2018). Recent studies have also explored the use of pervaporation and pressure-swing reactive distillation for systems containing azeotropes (Li et al., 2020; Li and Kiss, 2021; Wang et al., 2019). Beyond RD, dual RD has been demonstrated to exploit the

synergistic thermodynamic features that lead to a compact and efficient multiproduct unit (Dimian et al., 2009).

Invited for the Special Issue on *Advances in Bioprocess Intensification*, this original paper focuses on expanding the applicability of reactive distillation by exploiting synergies through further intensification by combining a dividing wall and two reactive zones in one vessel, namely a novel *dual reactive dividing wall column* (dual R-DWC). The choice of using an R-DWC was a development from existing flowsheets that feature a sequence of reactive distillation columns, where the dual function (two reactive sections) is implemented under the same operating pressure following a rule-based approach. The dual function uses a reversible reaction to improve the driving forces allows overcoming phenomenological limitations (high boiling points) of the initial separation through the forward reaction (Cardona Alzate et al., 2019). The reverse reaction is then used to recover the initial target molecules after the challenging separation has been accomplished. The reaction direction can be easily shifted by adjusting the liquid phase concentrations following the Le Chatelier's principle. The application of the dual R-DWC can be evaluated for fluid chemical systems that feature multiple outlet process streams (products, impurities, excess water, mass separating agent) and the need for the forward and reverse reactions (e.g., esterification-hydrolysis). In principle, the methodology developed in this research can be applied to evaluate chemical systems that are suitable for RD, i.e., equilibrium-limited systems where the reactions take place in the liquid phase only. This research is demonstrated through a special case study where a reversible reaction is introduced to facilitate the initial separation problem: the purification of lactic acid (LA) from a dilute aqueous mixture with low-concentration impurities that exhibit similar physicochemical behaviour.

This paper is the first to carry out the synthesis and conceptual design of a process flowsheet based on an intensified dual R-DWC, which is at the center of an industrial case study for the concentration and purification of a dilute aqueous stream of lactic acid (LA) from a fermentation broth. From a process design viewpoint, previous studies have overlooked the effects of impurities in the process performance, as process simulation research to date has not yet considered the effect of reactive impurities in the concentration of LA and used simplified fermentation broths as detailed in section 2.4. Therefore, this investigation accounts for the impact of succinic acid (SA) as a heavy reactive impurity on the purification of LA. The methodology follows a ruled-based approach that includes a synthesis procedure through a decomposition approach and the process' conceptual design using shortcut models and rigorous simulations in Aspen Plus V8.8. Also, an energy integration analysis is performed to

find additional opportunities for heat recovery. Finally, a brief assessment using sustainability metrics is carried out, and the results are directly compared against the benchmark studies reported in previous articles.

2. Case study: Downstream processing of lactic acid

The application of a methodology to derive the intensified dual-reactive dividing wall column (dual R-DWC) is illustrated by a direct application to a case study. This section provides a general overview of lactic acid production, emphasising the last stages of preconcentration and purification along with the associated challenges, which are tackled by the proposed methodology. Also, the feed and product characteristics, the different approaches to handle impurities in lab-based and simulation-based studies, and the catalyst selection are addressed.

2.1 Lactic acid production process

Lactic acid (2-hydroxypropionic acid) is an α-hydroxy organic acid produced industrially for the first time, through the chemical route, in the United States. The chemical route limitations include high manufacturing costs and the inability to produce the desirable L-(+)-lactic acid stereoisomer (Datta and Henry, 2006). Figure 1 presents a block diagram of the conventional process for LA production. Most LA production processes are currently based on carbohydrate fermentation using microorganisms (Gruber et al., 2006). The microorganism's varying metabolism demand varying amounts and types of nutrients and produce fermentation by-products such as fumaric acid, acetic acid, succinic acid, and ethanol. As a result, the fermentation broth constitutes a complex mixture because of the non-reacted sugars, excess nutrients and byproducts, determining the downstream processing steps (Oliveira et al., 2019). The possible configurations of LA downstream processing strongly depend on the fermentation broth composition and the purity required. Datta and Henry (2006) recognised that the separation and purification of LA remain as the primary technology barriers due to the difficulty of removing salts formed during the fermentation stage, which poses a challenge to the final disposition options and generates an environmental liability.

The dotted box in Figure 1 envelops the focus of this case study: the preconcentration and purification steps. The preconcentration stage removes the bulk solvent to reduce the solution's volume by evaporation in a range between 10 % to 75 % wt. while limiting the loss of lactate material from 0.1 % to 1 %wt. (Mizrahi et al., 2006). Finally, the purification stage removes the remaining organic acid impurities by reactive extraction, adsorption, electrodialysis and esterification followed by reactive distillation. Among these purification

techniques, RD can successfully separate other organic acids from LA while simultaneously removing excess water (Joglekar et al., 2006; Komesu et al., 2017). The reaction of non-desired organic acids and alkyl alcohols into esters with different boiling points facilitates the separation via distillation (Qureshi et al., 2011). After the separation of the alkyl esters, the alkyl lactate hydrolyses back to the acid form. As a result, RD has been explored as a promising alternative to purify LA (Cho et al., 2008; Kim et al., 2017; Su et al., 2013). Yet, these studies assumed heavy impurities that are not reactive and thus easily removed, which is unrealistic. This study goes a step further by considering reactive impurities during the process synthesis and design.

2.2 Characteristics of the LA stream for the preconcentration stage

The composition of fermentation broths varies widely due to the type of carbon source, the pH, and the microorganisms used for fermentation. The typical concentration of lactate material in a fermentation broth varies between 8 to 15 % wt. (Mizrahi et al., 2006). The diluted acid mixture contains water, LA and other acids, including fumaric acid, formic acid, acetic acid, and succinic acid. For this investigation, a previously studied mixture containing succinic acid (SA) as an impurity (this time reactive) was selected to allow a fair comparison among conventional and intensified processes (Kim et al., 2017; Su et al., 2013).

2.3 LA product specifications

Among the group of the organic acids, LA constitutes a versatile chemical with applications in cosmetics, foods, pharmaceuticals, and industrial use with mass concentrations of typically 50 %, 80 %, 88 % and 93 % (Gruber et al., 2006; Musashino, 2020). An emerging application of LA in the form of lactide monomers and co-monomers in concentrations of 100 % wt. is the production of polylactic acid (PLA), a bio-based plastic with promising applicability to replace fossil-based plastics (Okano et al., 2014). The major global producers of LA and derivatives are: Corbion Purac (The Netherlands), Galactic S.A. (Belgium), Henan Jindan Lactic Acid Co., Ltd. (China), Jungbunzlauer AG (Switzerland), Musashino Chemical Laboratory, Ltd. (Japan), and NatureWorks LLC (USA) (ReportLinker, 2020).

This research focuses on the production of LA 88 % wt. for the food industry, which is the most used industrially. The product specifications are LA 88 % wt., where dilactic acid (Di-LA) can be present up to 4.4 % wt., methyl lactate (ML) <1 % wt. and the remaining is water.

2.4 Reactive impurities

The separation of organic acids from LA is challenging due to the similar behaviour that these substances exhibit. The difference in boiling points cannot be easily exploited as increasing the operating temperature may lead to thermal degradation. For these reasons, converting the acids into esters facilitates separation, as the boiling temperatures of the esters are lower than their corresponding organic acids. A literature survey about studies that evaluated LA purification revealed the contrasting approaches towards impurities and water content when performing experiments or process simulations. In general, lab-based experiments evaluated the purification of LA using either fermentation broths or synthetic mixtures that account for impurities. In contrast, process simulation experiments use mixtures of LA and water only, in some cases also adding inert impurities.

Laube et al. (2016) studied the purification of LA experimentally from fermentation broths with impurities. As a result, a 15-unit operation process without reaction was produced, which did not effectively remove pyroglutamic acid, which is undesirable, especially for LA polymerisation into PLA. Uono (2013) focused on synthesising high purity lactate from a solution that contained organic components as impurities. The author claims that salting out with acetone allowed the removal of impurities, but no values indicating the initial and final concentrations are provided. Khunnonkwao et al. (2012) studied LA's purification from a fermentation broth containing reactive acetic acid. This study focused mostly on membrane design, but there is no mention of the separation effectiveness. Benedict et al. (2006) carried out various tests for LA and SA's co-processing for ester production, evaluating catalyst and membrane suitability. The process used a batch catalytic reactor followed by a pervaporation-assisted distillation. However, the synthetic mixtures contained little or no water and a large excess of ethanol, which are not realistic conditions for industrial application.

The simulation-based studies focusing on the techno-economic evaluation of LA production dismissed the presence of impurities (Dai et al., 2018; Gasca-González et al., 2019; Komesu et al., 2015). Other researchers have focused on the preconcentration and purification of LA, and they have considered the presence of high-boiler components (SA, Di-LA, Tri-LA) that do not react and are easily removed (Cho et al., 2008; Kim et al., 2017; Su et al., 2013).

Additional studies about the separation of mixtures of organic acids that showed relevant results for this research include the work of Orjuela et al. (2011), who studied, experimentally and in simulation, the separation of a mixture of succinic acid and acetic acid. This study showed the challenges and operating issues when dealing with a separation of organic acids. For example, the treatment of highly diluted mixtures (which resembled a fermentation broth)

showed low conversion, so they were not evaluated further by simulation. In addition, the unreacted SA precipitated and obstructed the outlet line of the cooled bottom product. Boontawan (2012) studied a vapour-permeation assisted esterification of a mixture of acids containing formic acid, acetic acid and LA with ethanol. All acids were converted into esters and then separated in a conventional distillation column. While the experimental studies demonstrate that the esterification with alcohol is not selective of the target acid, the simulation studies tend to dismiss this fact by simplifying the model. These experiences suggest that it is actually important to consider the impact of reactive impurities in the process performance. This study offers a more realistic approach by considering a heavy reactive impurity (succinic acid) as part of the LA feed to be purified in order to evaluate its impact.

2.5 Catalyst selection

Previous experimental studies about the esterification of LA have tested a range of cation exchange resins including Amberlyst 15, Amberlyst XN-1010, D001, D002, and NKC (Benedict et al., 2006; Kumar et al., 2006; Sanz et al., 2004; Zhang et al., 2004). However, most kinetic studies have focused on the catalyst's characterisation, and not much attention has been paid to RD's operational constraints given by the device's mechanical and thermal limits. As a result, selecting a suitable catalyst is mostly guided by the chemical performance only.

Amberlyst 15 is widely used for LA research in RD (Dai et al., 2018; Gasca-González et al., 2019; Kim et al., 2017; Su et al., 2013). For example, Su et al. (2013) set the maximum operating temperature of the catalyst of 120 °C as a constraint for the reactive section in an RD column. Indeed, this setting limits the operating window due to equipment constraints and hinders the reaction. To overcome this limitation, we introduced Amberlyst 36 as a solid / heterogeneous catalyst to give a broader range of operation up to 150 °C with a mass density of 800 kg/m^3. This cationic resin catalyst exhibits a capacity of 5.40 eq/kg (i.e. the concentration of acid sites), while Amberlyst 15 presents a capacity of 4.70 eq/kg (Dupont, 2019). Therefore, this catalyst's performance can be considered at least as good as Amberlyst 15, and the kinetic data available is used in this work.

3. Modelling and simulation basis

This study uses a combination of equilibrium and rate-based models that account for the vapour-liquid equilibrium (VLE) and kinetics, respectively. The application of equilibrium and non-equilibrium models to describe R-DWC behaviour has been successfully validated

against pilot-scale experimental data, which provides confidence in the approach followed in this investigation (Egger and Fieg, 2019). However, the availability of accurate vapour-liquid equilibrium (VLE) data and kinetics is somewhat limited. Therefore, the selection and validation of the property model data and kinetics are described hereafter.

3.1 Property model

The property model needs to account for non-ideal behaviour and to handle consistently the phenomena associated with the presence of polar compounds (water, MeOH) and carboxylic acids (LA and SA), such as the solvation and the dimerisation in the vapour phase of carboxylic acids. The UNIQUAC-HOC and NRTL-HOC property models are adequate for chemical systems that feature non-idealities and strong interactions between acids in the vapour phase. However, to avoid introducing new variables that may impact the comparison with the previously published benchmark studies, the UNIQUAC-HOC model was selected.
Only four pairs were gathered from built-in databanks in Aspen Plus v8.8, using experimental data from the Dortmund databanks (LA-Water, Water-MeOH, Water-SA, Water-ML), while the remaining pairs were estimated using the UNIFAC method in Aspen Plus. Therefore, proper model validation was carried out using experimental data available in the literature – this is presented in the *Supplementary Information*.

3.2 Chemistry and kinetics

In the present study, the concept of '*reactive separating agent*' (RSA) is used for a compound to aid the separation through the reaction with the target component. This concept is analogous to the '*mass separating agent*' (MSA) and '*energy separating agent*' (ESA) that are used to aid separation by physical means only (Seider, 2017). Methanol (MeOH) was selected as the RSA based on the study of Su et al. (2013), which found that the MeOH system offered the lowest TAC as the flowsheet exhibited the fewest columns and produced the lightest lactate. In this manner, an equilibrium-limited and reversible reaction of the target components with an RSA could effectively remove impurities and recover the original purified compound through the reverse reaction. Consequently, the chemical system evaluated in this study consisted of eight components: the ones in the initial mixture and the reactions' products. Equations (1) to (5) illustrate the reactions included in the model.

$$\text{Lactic Acid (LA)} + \text{Methanol (MeOH)} \rightleftharpoons \text{Methyl Lactate (ML)} + \text{Water} \quad (1)$$

$$\text{Succinic Acid (SA)} + \text{MeOH} \rightleftharpoons \text{Monomethyl Succinate (MMS)} + \text{Water} \quad (2)$$

$$\mathrm{MMS} + \mathrm{MeOH} \rightleftharpoons \mathrm{Dimethyl\,Succinate\,(DMS)} + \mathrm{Water} \quad (3)$$

$$2\,\mathrm{LA} \rightleftharpoons \mathrm{Dilactic\,Acid\,(Di-LA)} + \mathrm{Water} \quad (4)$$

$$(\mathrm{Di-LA}) + \mathrm{LA} \rightleftharpoons \mathrm{Trilactic\,Acid\,(Tri-LA)} + \mathrm{Water} \quad (5)$$

The kinetic data for the esterification of LA with MeOH using Amberlyst 15 was obtained from the study of Sanz et al. (2004). The side reactions of SA with MeOH (Amberlyst 15) and the oligomerisation of LA (Dowex DR-2030) were gathered from the studies of Dudáš et al. (2014) and Asthana et al. (2006), respectively. A regression was applied to the experimental points to calculate the kinetic parameters. When no data points were available for the reverse reaction, the chemical equilibrium constant was used to calculate the 'pre-exponential factor of the reverse assuming that the activation energy is the same for both reactions. All the data sets were fitted to a pseudo-homogeneous kinetic model. The kinetic parameters for reactive distillation in Aspen Plus use a built-in power law expression, and the units depend on the basis selected for the holdup, which can be specified in terms of volume, mass or moles in the RadFrac module. The holdup basis selected in this study was the mass of catalyst per stage (which is 10 kg for esterification, and 12-14 kg for hydrolysis, assuming a catalyst occupancy of max 50 % of the holdup volume), so the corresponding units for the pre-exponential factor are expressed per mass of catalyst (e.g. $2.14 \cdot 10^4$ kmol/s$\cdot$kg$_{cat}$ for LA esterification) (Luyben, 2013). The catalyst bulk density (800 kg/m^3) allows converting the pre-exponential factor into a catalyst volume-based unit (e.g., $1.712 \cdot 10^7$ kmol/s$\cdot$m^3). The details of each set of data and the calculated kinetic parameters are presented in Table 1.

4. Research approach

The synthesis and conceptual design of an intensified flowsheet followed a ruled-based approach (e.g., analysing boiling points to select operating pressure, composition in the liquid phase) to drive the decisions to find opportunities for intensification and achieve performance improvement. The analysis and verification of each step of the synthesis and design used a combination of tools: a decomposition approach, shortcut calculations, rigorous simulation, and heat integration to achieve intermediate and final performance targets initially set in the scope of this conceptual design study. The assumptions of the proposed methodology include: no pressure drop across the columns, reaction in the liquid phase only, ideal mass transfer so an equilibrium model is used to describe mass transport between the liquid and vapour phases, kinetically controlled reaction described by a pseudo-homogenous kinetic model, reactive impurities that introduce additional components to the separation, fully-thermally

coupled configuration equivalent to DWC (as negligible heat transfer occurs through the wall), and multiple outlet streams with one product stream on specification. The results allowed a better understanding of the process and an evaluation using sustainability indicators, such as material intensity, E-factor, energy intensity, water consumption and the associated CO_2 emissions.

4.1 Decomposition approach applied to a dual reactive system

The decomposition approach was used to identify the individual tasks (functions) required for the reaction-separation problem: esterification, hydrolysis, rectifying and stripping. The esterification section carries out the forward reaction and converts LA and SA into their corresponding esters with lower boiling points. The stripping sections remove high-boiling components, while the rectifying sections drive the light components as overheads. Lastly, the hydrolysis section carries out the reverse reaction and converts the ML into LA. For this case study, the heaviest cut is removed in the first section of the arrangement, where the indirect sequence leads to a side-stripper configuration with a dual reactive function: esterification and hydrolysis. Then, these sections were coupled by placing the inlet, outlet and internal flows to drive the reactions (esterification or hydrolysis) and the separation, as shown in Figure 2. A detailed description of the approach applied to a dual reactive system is provided in the *Supplementary Information*.

4.2 Shortcut calculation and initialisation values

The shortcut calculations consisted of mass balances applied around different system boundaries to obtain initialisation values for a rigorous simulation. The sections identified through the decomposition approach were grouped such that only one reaction lies within the boundary or a key degree of freedom can be calculated (e.g., liquid split ratio, reflux ratio, boilup ratio), as shown in the dotted and dashed boxes in Figure 2. The outer system boundary contained all sections and targeted for the compositions of the top stream' containing MeOH and water and the product stream containing concentrated LA on specification. Next, three inner boundaries were considered around the esterification section, hydrolysis section and the rectifying section 2, where the latter featured the liquid split ratio at the top of the dividing wall that distributes the liquid between the two sections of the column (Yildirim et al., 2011). The composition of the liquid stream returning to the esterification section depends on the separation accomplished due to the VLE and the consumption and production rates on the second reactive section. Therefore, taking into account the reactions on the hydrolysis section

to calculate the composition of the returning liquid stream constitutes an adaptation of the methods for designing a DWC and an R-DWC with one reactive section (Mueller et al., 2007; Triantafyllou and Smith, 1992). A detailed description of the shortcut calculations performed around the different boundaries of the system is presented in the *Supplementary Information*. These shortcut calculations were fully automated in Excel, which facilitated recalculating values when accounting for non-sharp separations and partial conversion so that the operating parameters used to initialise the rigorous simulation account for a realistic system.

4.3 Rigorous simulation of the flowsheet and performance evaluation

Aspen Plus V8.8 was used to implement the flowsheet using the rigorous RadFrac module for the main units of the process. The process simulation results were used to calculate the key performance indicators and track various process variables.

Prior to implementing the novel dual reactive arrangement obtained from the decomposition approach, a preconcentration step was included to evaluate its performance in a full flowsheet. The preconcentration arrangement consisted of a heater, an expansion valve, and a flash vessel to promote an instantaneous separation of the feed into two phases: liquid and vapour. The flash vessel was set to operate adiabatically at atmospheric pressure (1 atm). The criterion to remove water in the preconcentrator followed two guidelines presented by Mizrahi et al. (2006): volume reduction from 10 % to 75 %wt. with a loss of LA between 0.1 to 1% wt. As the volume reduction allowed a wider variation range, only the LA loss was used as a design specification for the preconcentration arrangement, calculated with Equation (6). Sensitivity analysis was used to evaluate the effect of the outlet temperature from the heater on the LA concentration and flowrate of the solution for further processing, and the LA loss.

$$\text{LA loss} = \frac{\text{LA mass flowrate in the vapour stream}}{\text{LA mass flowrate in the feed stream}} * 100 \qquad (6)$$

The simulation of a dual R-DWC was performed using two RadFrac modules fully thermally coupled – a thermodynamically equivalent configuration, assuming that the mass-transfer resistances are equal and that the heat transfer through the wall is negligible (Novita et al., 2018). Figure 3 summarises the iterative procedure in a flowchart denoting four main activities: initialisation values adjustment, esterification column implementation, hydrolysis column implementation, and coupling. Several decision tasks within the main activity or to progress to the next activity checked simulation convergence and compliance with

intermediate and final targets set for the individual and coupled performance of the columns. The shortcut calculations (previously described) provided the initialisation values for the operating parameters (e.g., reflux ratio, bottom to feed ratio, boilup ratio, bottom rate), heuristics provided initialisation values for the design parameters (e.g., number of stages, feed location) and previous studies provided initialisation values for the catalyst holdup (e.g., 10 kg of catalyst per stage). The initial number of stages determined by heuristics was relatively large (30 stages per section: reactive, stripping, rectifying) (Al-Arfaj and Luyben, 2002). The feed streams to the esterification section were initially located at the two ends of the reactive section. Intermediate target values (e.g., conversion, desired split, target molecule losses) were set to fine-tune the number of stages following a sensitivity analysis procedure varying the catalyst holdup per stage, and the feed location and observing the temperature, composition and component generation profiles. Once the intermediate targets were met, the vapour stream leaving the esterification column was used as a feed stream to the hydrolysis column. The implementation of the hydrolysis column follows a similar initialisation procedure and fine-tuning until reaching the intermediate targets set (e.g., conversion, target molecule losses). Then, the returning stream leaving the hydrolysis section was updated in the esterification column following and iterative procedure until matching its composition and flowrate in the hydrolysis and esterification columns. Finally, the two columns were coupled and simulated to obtain the final target, which refers to the product specification. The *Supplementary Information* presents a detailed procedure to implement the dual R-DWC in Aspen Plus including the holdup variation, diameter sizing and convergence.

The distillate stream from the dual R-DWC contained excess water and MeOH, where the latter needs to be recovered and recycled so an additional distillation column is employed. Finally, the recycle stream was connected to the esterification section, and the simulation was satisfactorily run and converged. A detailed description of the implementation of the recovery column and the recycle stream is provided in the *Supplementary Information*.

Finally, the SPRINT software (v2.9), developed at the Centre for Process Integration (CPI) at the University of Manchester, was used to set energy targets and identify heat recovery opportunities (CPI, 2019). The mass and energy balances obtained from the rigorous simulation in Aspen Plus provided the stream data to be implemented in SPRINT. A minimum approach temperature of 10 K was selected, given the system's range of temperatures, and the utilities included in the analysis (see the *Supplementary Information*).

To complement the proposed flowsheet's technical evaluation, we assessed sustainability metrics such as material intensity, E-factor, energy intensity, water consumption and CO_2

emissions. The use of sustainability metrics can guide improvements in operations by enabling the comparison with benchmark processes, tracking improvement over time, or evaluating alternative processes for the manufacture of a given product, where the lower the metric, the more effective the process (Schwarz et al., 2002).

The material intensity was calculated as the ratio of mass of input materials (including water only when it constitutes part of the product) minus the mass of product(s) over the mass of products (product and byproducts) (Equation (7)). The E-factor accounts for the waste produced and it was calculated as the ratio of the mass of waste (excluding water) over the mass of product (Equation (8)) (Sheldon, 2018).

$$\text{Mass Intensity} = \frac{\text{mass of raw materials in} - \text{mass of final product}}{\text{mass of final product}} \quad (7)$$

$$\text{E factor} = \frac{\text{total mass of waste}}{\text{mass of final product}} \quad (8)$$

The energy intensity was calculated using the overall heat duty of the reboilers and heaters over the mass of LA product. The water consumption metric comprises the volume of freshwater consumed in the process and the losses of water due to evaporation or disposal over the mass of LA product (Equation (9)).

$$\text{Water consumption} = \frac{\text{fresh water inlet} + \text{losses from cooling} + \text{water disposed}}{\text{mass of final product}} \quad (9)$$

The CO_2 emissions associated with the preconcentration and purification steps were calculated based on the US-EPA-RULE-E9-5711 method, according to Equation (10). This calculation considered the consumption of hot utilities only, assuming the use of natural gas as a fuel for steam production (so fossil fuel instead of renewable sources). The CO_2 emission factor is fuel-dependent and uses a default oxidation factor of one, which assumes that all the carbon present in the fuel oxidises. The CO_2 emission factor for natural gas is $5.589 \cdot 10^{-8}$ kg CO_2/J. The energy source efficiency factor (*2006 IPCC Guidelines for National Greenhouse Gas Inventories*) assumes that the efficiency of the transformation of fuel to energy is higher than the efficiency of the transformation of fuel to electricity. The latter was not accounted for the downstream section under study. Thus, for this research, an efficiency factor used is 0.85. The CO_2 emissions metric is presented as the mass of CO_2 over the mass of the LA product.

$$\text{CO}_2\text{ emission rate} = \frac{\text{heat duty} * \text{CO}_2\text{emission factor}}{\text{energy source efficiency factor}} \quad (10)$$

5. Results and discussion

This section presents the results of each stage of the methodology and the analysis that drove the decisions made in the process synthesis and conceptual design journey. The results are organised as follows. Before the synthesis of potential processing options, the boiling points were analysed to select a suitable operating pressure. Then, a decomposition approach and the application of shortcut calculations informed the initialisation values to build a rigorous process flowsheet. Once a robust simulation offered the mass and energy balance results, the heat integration analysis and the sustainability metrics were calculated and evaluated.

5.1 Boiling point analysis and selection of operating pressure

The components of the original mixture and the reactions' products were listed in increasing boiling points order. Table 2 presents the boiling and azeotrope temperatures at different pressures (see extended dataset in *Supplementary Information*). The maximum operating temperature for the reaction zone – limited by the ' thermal degradation of the catalyst (150 °C) – and the decomposition temperatures of the components were included as constraints. Also, the process design aimed to use cooling water as a cheap cold utility.

The reactive zone must contain the reactants in close contact to achieve the esterification between LA and MeOH, while ML needs to be recovered in the overheads after being separated from the heavier compounds. Pressures below atmospheric are preferred to drive the ML to the top without compromising the catalyst's integrity. LA and SA's decomposition temperatures limit the bottom streams' temperature, suggesting again to operate at low pressure. Clearly, high vacuum favours the separation and avoids catalyst degradation, but lowered temperatures also hinder the reaction's progression (slow kinetics), and the top end of the column would require expensive cooling.

As the esterification reaction's purpose is to convert LA into ML, the first split aimed to produce an overhead product containing ML and lighter products, and a bottom stream of impurities, where ML and DMS were the light and heavy key components, respectively. However, azeotropes are possible between the two pure components. Thus, the temperature above the reactive section required to be at least at the boiling point of ML, while the higher boiling azeotropes are maintained in the reactive zone to drive the reaction of LA into ML and push the heavier components downwards. The additional heat of the exothermic reactions will raise the reactive section's temperature, so the temperature profile needs monitoring to avoid the catalyst degradation in the lower end of the reactive section.

There is a compromise between the temperature to favour the separation and the reaction. Figure 4a presents ML, MMS and DMS's production rates at different temperatures assuming an equimolar feed, where temperatures below 193 °C favour ML production over MMS and DMS. Figure 4b presents ML, MMS and DMS's production rates at different pressures and evaluated at the corresponding boiling temperature of ML. This figure shows that increasing operating pressure raises the production rates of all products. However, the distribution favours MMS and DMS over ML, which will affect the consumption of MeOH. Thus, the operating pressure that favours the esterification of LA, while keeping low the production rates of MMS and DMS, was 0.5 atm.

5.2 Decomposition approach insight into shortcut models and rigorous simulation

The shortcut calculations over the boundaries depicted in Figure 2 provided the initialisation values for flowrates and compositions of the outlet streams and operating parameters set as specifications. The *Supplementary Information* provides a block diagram and the shortcut calculations' results after evaluating a liquid split ratio of 0.4. Also, the bottom to feed molar ratio for inner boundary 1 was found to be B/F=0.017, and the reflux ratio for the inner boundary 3 was RR=0.92. These values are then used to initialise the rigorous simulation.

5.3 Rigorous simulation of the process flowsheet

5.3.1 Preconcentration of the fermentation broth

The sensitivity analysis (see Figure 5) evaluated the impact of the outlet stream temperature from the heater (manipulated variable) on the molar flowrate and the mass percentage of LA of the liquid stream for further processing. The analysis indicates that temperatures lower than 127 °C allowed maintaining the LA loss below the limit. A temperature of 126 °C was selected such that the LA loss corresponds to 0.69 % wt. and the flowrate reduction is approximately 40 %, which is in line with the specification suggested by Mizrahi et al. (2006). The vapour stream from the flash vessel contained mostly water with a low calorific value and provided heating making use of the latent heat available, which is further discussed in the energy integration section 5.4. The liquid stream continued to the purification step.

5.3.2 Dual esterification-hydrolysis dividing wall column and methanol recovery

Implementing a robust esterification column in Aspen Plus required additional setup parameters due to the complexity of the connections and interactions and new degrees of freedom. For example, the MeOH stream flowrate impacts the reaction and the reactive

section's temperature, which is constrained by the catalyst. With a stoichiometric feed ratio, the reaction zone temperatures were too high, which drove oligomers' high production rates. Thus, a sensitivity analysis was performed to find the MeOH to organic acids ratio that allows maintaining the reaction zone at temperatures below 150 °C. Figure 6 presents the reactive section's column profiles resulting from the sensitivity analysis of the feed molar ratio of MeOH to the organic acids, LA and SA. Notably, the stoichiometric feed ratio of one led to temperatures of up to 350 °C, exceeding the catalyst constraint and promoting oligomers' production. Figure 6d shows Di-LA's production in the first reactive stages and then the consumption leading to Tri-LA production, which degrades the material and reduces the recovery, as the oligomers are removed with a high-boiling fraction containing the impurities. Increasing the MeOH to organic acids ratio clearly reduced the temperature along the reactive section and hindered oligomers' formation. Thus, the MeOH makeup is an important degree of freedom that plays a key role in maintaining the reactive section's temperature and the subsequent oligomers production. These results also support the selection of a catalyst that withstands higher operating temperatures. The production rate profile for ML in Figure 6c shows that the reverse reaction occurred in the first two reactive stages as the LA feed was rich in water and promoted the reverse reaction, with ML produced in the lower stages of the reactive section. Thus, moving the LA feed two stages above the reactive section allowed the reaction to occur from the first reactive stage, as some of the water fed was dragged to the top of the column. Increasing the MeOH concentration in the liquid phase with increasing molar feed ratio favoured the esterification reaction, as presented in Figure 6b.

The condenser was removed once a relatively constant temperature along the reactive section is obtained by simulation. Then, a new degree of freedom must be considered: the liquid split ratio that dictates the incoming liquid stream required in the column. The returning stream composition was set using the information from the shortcut calculations, and the flowrate was evaluated in a sensitivity analysis with different split ratios, presented in Figure 7.

As a result, the higher the split towards the esterification section, the higher the reboiler duty due to the increased volume returned. However, the remaining parameters showed a minimum temperature (top and bottom) and Di-&Tri-LA molar fraction; and a maximum conversion and impurities removal using a split ratio of 0.2, which is used to build a base case. Small discrepancies are attributed to the adjustment needed in the manipulable operating parameter (bottom to feed ratio) to align with the mass balance and subsequent convergence. Therefore, a liquid split ratio of 0.2 towards the esterification column was selected to continue building the simulation. Further optimisation of the liquid split ratio could be explored in the vicinity

this value following a multi-objective optimisation procedure beyond the conceptual design in the scope of the proposed methodology. The *Supplementary Information* presents detailed information on the setup parameters and results to obtain a robust esterification column simulation.

The implementation of the hydrolysis column in a RadFrac module used the initialisation values from the shortcut calculations and simulation results from the esterification column. Figure 8 shows the profiles of the composition of the liquid phase and the production rates per stage. The analysis of both profiles is quite revealing in several ways. First, in Figure 8a, it is evident that most ML, once fed, travelled upwards without contacting the catalyst. Second, the high ML concentration compared to the MeOH concentration above the reactive section also indicated the low hydrolysis reaction's rates. In addition, the concentration of water in the liquid phase, which is not depicted, was sufficiently high to guarantee the reaction's occurrence. Thus, the inlet and returning stream locations were systematically lowered in the reactive section so that the ML conversion improves and the ML loss in both ends of the column is reduced. Nevertheless, a compromise should be made between the increase in conversion and the ML concentration in the bottom stream, as the feed stream moves downwards, the bottom stream is also enriched in this component. Figure 8c shows the improved case where the number of reactive and striping stages and the catalyst holdup have been adjusted.

Coupling the esterification and hydrolysis columns in Aspen Plus required several iterations until reaching the targets set for each column's operation and the product specifications, as described in the flowchart of Figure 3. The final step to complete the simulation of the dual R-DWC required the implementation of the recycle stream after the simulation of the recovery unit'. Table 3 provides details about the setup parameters for esterification and hydrolysis columns, and the intermediate and final targets for the base case (before coupling), thermally coupled columns after integration and the configuration including the recycle stream. The iterations that led to significant changes in the parameters occurred when coupling both columns. Then, once the recycle stream was calculated and implemented, the MeOH makeup flowrate was the one that required substantial adjustment, which was defined by the design specification to keep the reactive section at < 150 °C. The intermediate targets defined for the esterification section included LA conversion > 99 %, near-sharp ML-DMS split and LA loss < 1 %. The LA conversion and ML-DMS split were easily achieved. The LA loss in the bottom stream was reduced with the adjustments carried out in the number of stages and feed location. For the hydrolysis section, the intermediate targets included ML conversion > 80 %

and ML loss in the top and bottom streams < 2 %. The base case presented a low conversion of methyl lactate as some material exits the column to enter the esterification section. Once coupled, the location of the inlet and side-draw streams' and the catalyst holdup adjustment allowed reaching higher conversion and reduced the loss of ML from both ends of the hydrolysis section.

5.3.3 Mass balance and key parameters

Figure 9 presents the process flowsheet for the preconcentration and purification of LA, and the key stream-data and design features. First, the diluted LA entered a flash vessel (V-1) arrangement, including a heater and a valve. The water-rich vapour stream provided low-grade heat to be recovered, while the preconcentrated LA liquid stream entered the esterification column (C-1). The impurities were removed in the bottom stream of C-1. The ML-rich stream was then fed to the reactive section in the hydrolysis column (C-2) while a liquid side-draw entered the top of C-1. The LA product was removed from the bottom of C-2. The distillate stream from C-2 entered a distillation column (C-3) to remove excess water and recover MeOH.

5.4 Heat integration of the flowsheet

Figure 10 presents the composite curves of the process, where the blue curve represents the cold composite curve, and the red curve represents the hot composite curve. The overlap between the two curves denotes that the heat available for process-to-process recovery was 267.7 kW, which resulted in a reduction of hot and cold utilities of 17 % and 22 %, respectively. The minimum cold utility (cooling water) corresponds to 1177.3 kW, and the minimum hot utility accounts for 1280.3 kW (distributed in 853.3 kW of low-pressure steam and 427 kW of high-pressure steam). The initial conditions and design constrain the heat recovery (e.g., feed condition for downstream, flash vessel pressure). However, the flash vessel pressure selected could bring benefits of reducing capital and operating costs due to using standard operating conditions.

5.5 Sustainability metrics

The process's sustainability was evaluated using several metrics proposed by industrial experts: material intensity, E-factor, energy intensity, water consumption, and CO_2 emissions. These values allow comparing the operations performance with benchmark processes, with lower values meaning better performance.

5.5.1 Material intensity

This metric indicates the input materials used per unit of output. The inlet streams to the process are LA in the diluted feed = 376.6 kg LA/h, SA in the diluted feed = 62.7 kg SA/h, the MeOH makeup = 26.1 kg MeOH/h and the water fed that is intended to be part of the product (12 % wt.) that corresponds to 51.4 kg water/h (376.6×12/88), and the product (output) corresponds to 411.3 kg/h of LA (88 % wt.). The impurities stream is a mixture of SA, MMS and DMS that is not considered a co-product. As a result, the material intensity of the proposed flowsheet is 0.256 kg_{input}/kg LA product. Note that the calculation of material intensity for the benchmark studies (Section 5.6) featured an additional input: the water used for the hydrolysis of methyl lactate accounted stoichiometrically, and the implications will be discussed accordingly.

5.5.2 E-factor

The E-factor gives an indication of the waste produced in the process. The waste stream corresponds to the impurities containing SA and its corresponding esters, MMS and DMS, and is equal to 73.3 kg/h. The E-factor for the proposed flowsheet is 0.178 kg_{waste}/kg LA. It is important to note that by considering the SA as a reactive impurity, the esters produced have a higher molecular weight and consume part of the MeOH fed to the process. To reduce the waste produced, the impurities stream could be upgraded into DMS for applications such as flavouring agent, paint additive, pigment solvent and viscosity adjustor (Seqens, 2021).

5.5.3 Energy intensity

Energy intensity is a measure of the primary energy consumed per unit of output, considering the heat duty of reboilers and heaters. The energy intensity for the process proposed here is 13.5 MJ/kg LA product before indirect heat integration (base case), and 11.2 MJ/kg LA product (including heat recovery).

5.5.4 Water consumption

This metric indicates the freshwater consumed per unit output, which accounts for the freshwater inlet, losses from cooling, and water disposal. One of the major realisations of the proposed flowsheet was the reuse of the water produced in the esterification section to carry out the hydrolysis reaction. Therefore, no additional freshwater was introduced to the system. The evaporation losses were estimated as 7 % of the cooling water (Schwarz et al., 2002). The

cooling water flowrate was computed from the cooling duty once heat integration was introduced (1135.2 kW), and the cooling capacity of water was 20.9 kJ/kg given by the supply and return temperatures of cooling water, 25 °C to 30 °C. Therefore, the loss by evaporation of cooling water corresponds to 13.7 m^3/h. The proposed flowsheet features two outlet water streams containing low concentrations of LA (from the preconcentrator) and ML and MeOH (from the recovery column) that add up to 0.80 m^3/h. The low concentrations and volume (relative to the makeup of cooling water needed) enable the water reuse in usual water sink options such as cooling water makeup and boiler feedwater (Eslamian, 2016; Quaglia et al., 2014). In a biorefinery, potential water sinks are medium preparation for fermentation, pretreatment such as enzymatic hydrolysis (Abdelaziz et al., 2015; Murphy et al., 1982). Hence the water consumption for the proposed process is only 0.033 m^3 water/kg LA product.

5.5.5 CO_2 emissions

The CO_2 emissions are expressed as the mass of CO_2 emitted due to the combustion of natural gas for steam production (heating duty), as previously explained in section 4.3 and the Equation (10), over the product mass. The base case's CO_2 emission rate (without heat integration) was 366 kg CO_2/h (for a production capacity of 3.5 ktpy of LA product), and the corresponding CO_2 emissions were 0.89 kg CO_2/kg LA product. Evidently, the introduction of indirect heat integration reduced the emissions rate to 280 kg CO_2/h, and the CO_2 emissions per unit output were reduced to 0.68 kg CO_2/kg LA.

5.6 Comparison with previous studies

The comparison between the flowsheet presented in the previous sections and the available benchmark studies was not straightforward due to additional features considered during the synthesis and conceptual design of the novel processing unit. These additional features were the reaction of the impurity (i.e., SA esterification) and higher temperature-limit for the reactive zone than that of the benchmark studies (120 °C) due to using a catalyst that withstands up to 150 °C. However, the results presented and discussed hereafter provide an indication of the potential of the novel configuration using technical and sustainability indicators. Table 4 shows the key performance indicators selected to evaluate the flowsheet's behaviour, including the dual R-DWC and the benchmark studies.

The MeOH makeup flowrate found in this work was four times higher than the flowrate of the benchmark studies. This increase is attributed to the esterification of SA that consumes MeOH to produce MMS and DMS, where the latter are removed with the impurities stream,

so MeOH cannot be recovered. This finding provides additional arguments in favour of the hypothesis posed that reactive impurities impact the separation of lactic acid, which has been overseen in previous studies. The additional MeOH (0.05 kg MeOH/kg LA) may impact the raw materials' costs and suggest a point worth to be considered even at an early design stage. Further developments beyond the conceptual design could include a formal multi-objective optimisation procedure to target an overall performance variable (e.g., energy usage, total annual cost) making use of adequate cost correlations that account for non-conventional configurations. Meanwhile, the material intensity metric showed the lowest value for the proposed flowsheet despite the increased MeOH makeup (28-32 % reduction) because of the elimination of additional water required to perform the hydrolysis reaction by using the water produced in the esterification reaction. This outcome was achieved by appropriately placing the vapour stream from the esterification section in the hydrolysis section so that the water required for the reaction was available in the liquid phase. The E-factor presented an increase of 10-11 % suggesting that the proposed flowsheet produced a larger amount of waste due to the production of MMS and DMS, which feature high molecular weights. Yet, this apparently inferior performance corroborates the hypothesis that accounting for reactive impurities, even at low concentrations, can give a more realistic indication of the operating costs (i.e., additional raw materials) and the environmental performance (i.e, waste produced).

The feed stream to purification contained a similar LA amount, but this study showed a higher water amount. The benchmark studies used a conventional distillation column operating at 0.1 atm to remove approximately 88 % of water, while this work used a flash drum at 1 atm and achieved 60 % removal. Although the water removal was not as good, introducing a flash vessel made it possible to recover some low-grade heat contributing to reducing the overall energy use of the proposed flowsheet (reduction of 17 % hot utility, and 22 % cold utility). Regarding the energy used, the process-to-process heat integration reduced the heating duty by 27 % and 13 % compared to the benchmarks, respectively. This result is also reflected in the energy intensity metric, where the proposed flowsheet presents the best performance.

The apparent lower capacity of the proposed flowsheet (0.54 to 2.15 % reduction) is due to the lower Di-LA content, which has a higher molecular weight, in the LA product. All products comply with the Di-LA limit of 4.4 % wt., but our flowsheet achieved a higher LA recovery than the benchmark studies. This result is explained by the fact that milder temperatures in the hydrolysis section reduced oligomerisation reactions, thus avoiding Di-LA formation, which is a form of degradation of our target molecule.

The MeOH to LA feed molar ratio in this study is the lowest, even though the amount of water entering the first column is high. This result could be attributed to the catalyst that withstands higher temperatures, so less MeOH was required to quench the reactive section.

The water consumption metric for the proposed flowsheet presents a reduction of 36 % and 22 % compared to the benchmark studies. The three principal contributions for reducing the water consumption were the lower water makeup required due to the evaporation losses (lower cooling duty), the potential reuse of the outlet water streams (e.g., cooling water makeup, boiler feedwater, medium preparation for fermentation) and the elimination of the freshwater stream to the hydrolysis section.

The total CO_2 emissions associated to the conventional sequence columns presented in the work of Su et al. (2013) was 1.01 kg CO_2/kg LA, and for the flowsheet including the fully thermally coupled column in the study of Kim et al. (2017) was 0.83 kg CO_2/kg LA. The process proposed in this work, without and with heat recovery has figures of 0.89 kg CO_2/kg LA and 0.68 kg CO_2/kg LA, respectively. Evidently, the introduction of direct heat integration in the dual R-DWC and the process-to-process indirect heat integration allowed reducing the CO_2 emissions, which positively impacted the ecological footprint.

6. Conclusions

The new methodology proposed here for the synthesis and conceptual design of a dual R-DWC was successfully demonstrated and used in an industrially relevant case study about the downstream processing of bio-produced lactic acid. The methodology followed a rule-based approach and included a combination of a decomposition method, shortcut models and rigorous simulations to obtain a robust flowsheet in which the heat recovery opportunities were fully explored and exploited. The decomposition procedure allowed the identification of the fundamental tasks that must be performed in the process, while the process synthesis and conceptual design combined these tasks effectively to generate a further intensified unit, namely a dual R-DWC that features both the forward and reverse reactions and the separation in one vessel.

Further development of the methodology is ongoing to derive a systematic approach to expand the range of processing options beyond R-DWC to synthesise advanced reactive distillation technologies. Although further case studies are yet to be carried out, the proposed approach could be evaluated in biorefinery applications for the purification of organic acids via esterification (e.g. citric acid, succinic acid, propionic acid), and the production of esters via hydrolysis or transesterification (e.g. methyl acetate, ethyl acetate, fatty alkyl esters).

Even at an early design stage, accounting for realistic and challenging characteristics (e.g., highly diluted feeds, reactive impurities) revealed the possible implications for the economics and technical feasibility when evaluating detailed designs and optimising in terms of energy usage, total annual cost, capital cost or operating cost. For example, the presence of reactive impurities in the mixture to be purified must be accounted for, as more byproducts are formed, and more raw materials are used (compared to less realistic studies based on simplified assumptions), which makes the downstream processing more complex.

The novel dual R-DWC was evaluated using sustainability metrics, which also allowed a fair comparison against benchmark processes reported in the literature. The results show that the novel dual R-DWC process proposed in this study improves sustainability, as reflected by key metrics: energy intensity of 11.2 MJ/kg LA (savings of 11-27 % vs benchmarks), material intensity of 0.256 kg_{input}/kg LA (28-32 % reduction), water consumption of 0.033 m^3/kg LA (reduction of 22-36 %), and CO_2 emissions of 0.68 kg CO_2/kg LA (reduction of 18-33 %).

Acknowledgement

AAK gratefully acknowledges the Royal Society Wolfson Research Merit Award (No. WM170003). IPM gratefully acknowledges the full fund support from SENESCYT-Ecuador.

Abbreviations

LA	Lactic acid
SA	Succinic acid
MeOH	Methanol
ML	Methyl lactate
MMS	Monomethyl succinate
DMS	Dimethyl succinate
Di-LA	Dilactic acid
Tri-LA	Trilactic acid
PI	Process intensification
RD	Reactive distillation
R-DWC	Reactive dividing wall column
R-HiGee	Reactive high-gravity distillation
CCD	Catalytic cyclic distillation
R-HIDiC	Reactive heat-integrated distillation column
MA-RD	Membrane-assisted reactive distillation
VLE	Vapour-liquid equilibrium
UNIQUAC-HOC	Universal Quasichemical model with Hayden-O'Connell correction
NRTL-HOC	Non-Random Two liquid model with Hayden-O'Connell correction
RSA	Reactive separating agent
MSA	Mass separating agent
ESA	Energy separating agent
TAC	Total annualised cost

B/F	Bottom-to-feed molar ratio
RR	Reflux ratio
LS	Liquid split ratio

References

1. Abdelaziz, O.Y., Gadalla, M.A., El-Halwagi, M.M., Ashour, F.H., 2015. A hierarchical approach for the design improvements of an Organocat biorefinery. Bioresour. Technol. 181, 321–329. https://doi.org/10.1016/j.biortech.2015.01.068
2. Al-Arfaj, M.A., Luyben, W.L., 2002. Comparative control study of ideal and methyl acetate reactive distillation. Chem. Eng. Sci. 57, 5039–5050. https://doi.org/10.1016/S0009-2509(02)00415-3
3. Alves de Oliveira, R., Komesu, A., Vaz Rossell, C.E., Maciel Filho, R., 2018. Challenges and opportunities in lactic acid bioprocess design—From economic to production aspects. Biochem. Eng. J. 133, 219–239. https://doi.org/10.1016/j.bej.2018.03.003
4. Asthana, N.S., Kolah, A.K., Vu, D.T., Lira, C.T., Miller, D.J., 2006. A Kinetic Model for the Esterification of Lactic Acid and Its Oligomers. Ind. Eng. Chem. Res. 45, 5251–5257. https://doi.org/10.1021/ie0513604
5. Benedict, D.J., Parulekar, S.J., Tsai, S.-P., 2006. Pervaporation-assisted esterification of lactic and succinic acids with downstream ester recovery. J. Membr. Sci. 281, 435–445. https://doi.org/10.1016/j.memsci.2006.04.012
6. Boontawan, A., 2012. Purification of Succinic Acid from Synthetic Solution Using Vapor Permeation-Assisted Esterification Coupled with Reactive Distillation. Trans Tech Publications 550–553, 3008–3011. https://doi.org/10.4028/www.scientific.net/AMR.550-553.3008
7. Cardona Alzate, C.A., Ortiz Sanchez, M., Pisarenko, Y., 2019. Reactive Separation for Process Intensification and Sustainability. CRC Press. https://doi.org/10.1201/9780429300387
8. Chahal, S.P., 2000. Lactic Acid, in: Ullmann's Encyclopedia of Industrial Chemistry. American Cancer Society. https://doi.org/10.1002/14356007.a15_097
9. Cho, Y., Kim, B., Kim, Dongpil, Han, Myungwan, 2008. Recovery of lactic acid by reactive dividing wall column. Presented at the 2008 International Conference on Control, Automation and Systems, pp. 2596–2599. https://doi.org/10.1109/ICCAS.2008.4694294
10. CPI, 2019. Software packages - Centre for Process Integration - The University of Manchester [WWW Document]. URL https://www.ceas.manchester.ac.uk/cpi/research/resources/software/ (accessed 10.14.20).
11. Dai, S.-B., Lee, H.-Y., Chen, C.-L., 2018. Design and Economic Evaluation for Production of Ethyl Lactate via Reactive Distillation Combined with Various Separation Configurations, in: Eden, M.R., Ierapetritou, M.G., Towler, G.P. (Eds.), Computer Aided Chemical Engineering, 13 International Symposium on Process Systems Engineering (PSE 2018). Elsevier, pp. 127–132. https://doi.org/10.1016/B978-0-444-64241-7.50016-1
12. Datta, R., Henry, M., 2006. Lactic acid: recent advances in products, processes and technologies — a review. J. Chem. Technol. Biotechnol. 81, 1119–1129. https://doi.org/10.1002/jctb.1486
13. Dimian, A.C., Bildea, C.S., Omota, F., Kiss, A.A., 2009. Innovative process for fatty acid esters by dual reactive distillation. Comput. Chem. Eng., Selected Papers from

the 17th European Symposium on Computer Aided Process Engineering held in Bucharest, Romania, May 2007 33, 743–750. https://doi.org/10.1016/j.compchemeng.2008.09.020
14. Dudáš, J., Kotora, M., Bradáč, M., Markoš, J., 2014. Design consideration of dimethyl succinate production process. Chem. Pap. 68, 1667–1677. https://doi.org/10.2478/s11696-014-0580-4
15. Dupont, 2019. AmberLyst^{TM} Polymeric Catalysts.
16. Egger, T., Fieg, G., 2019. Operation, validation and model comparison for a reactive dividing wall column. Chem. Eng. Sci. 207, 993–1006. https://doi.org/10.1016/j.ces.2019.07.032
17. Eslamian, S., 2016. Urban Water Reuse Handbook. CRC Press.
18. Gasca-González, R., Prado-Rubio, O.A., Gómez-Castro, F.I., Fontalvo-Alzate, J., Pérez-Cisneros, E.S., Morales-Rodriguez, R., 2019. Techno-economic analysis of alternative reactive purification technologies in the lactic acid production process., in: Kiss, A.A., Zondervan, E., Lakerveld, R., Özkan, L. (Eds.), Computer Aided Chemical Engineering, 29 European Symposium on Computer Aided Process Engineering. Elsevier, pp. 457–462. https://doi.org/10.1016/B978-0-12-818634-3.50077-1
19. Gorak, A., Stankiewicz, A., 2018. Intensification of Biobased Processes. Royal Society of Chemistry.
20. Gruber, P., Henton, D.E., Starr, J., 2006. Polylactic Acid from Renewable Resources, in: Biorefineries-Industrial Processes and Products. John Wiley & Sons, Ltd, pp. 381–407. https://doi.org/10.1002/9783527619849.ch31
21. Joglekar, H.G., Rahman, I., Babu, S., Kulkarni, B.D., Joshi, A., 2006. Comparative assessment of downstream processing options for lactic acid. Sep. Purif. Technol. 52, 1–17. https://doi.org/10.1016/j.seppur.2006.03.015
22. Khunnonkwao, P., Boontawan, P., Haltrich, D., Maischberger, T., Boontawan, A., 2012. Purification of l-(+)-lactic acid from pre-treated fermentation broth using vapor permeation-assisted esterification. Process Biochem. 47, 1948–1956. https://doi.org/10.1016/j.procbio.2012.07.011
23. Kim, S.Y., Kim, D.M., Lee, B., 2017. Process simulation for the recovery of lactic acid using thermally coupled distillation columns to mitigate the remixing effect. Korean J. Chem. Eng. 34, 1310–1318. https://doi.org/10.1007/s11814-017-0009-1
24. Kiss, A.A., 2017. 4. Process intensification by reactive distillation, in: Process Synthesis and Process IntensificationMethodological Approaches. De Gruyter, Berlin, Boston. https://doi.org/10.1515/9783110465068-004
25. Kiss, A.A., Jobson, M., Gao, X., 2019. Reactive Distillation: Stepping Up to the Next Level of Process Intensification. Ind. Eng. Chem. Res. 58, 5909–5918. https://doi.org/10.1021/acs.iecr.8b05450
26. Komesu, A., Maciel, M.R.W., Oliveira, J.A.R. de, Martins, L.H. da S., Filho, R.M., 2017. Purification of Lactic Acid Produced by Fermentation: Focus on Non-traditional Distillation Processes. Sep. Purif. Rev. 46, 241–254. https://doi.org/10.1080/15422119.2016.1260034
27. Komesu, A., Martins, P.F., Lunelli, B.H., Oliveira, J., Filho, R.M., Maciel, M.R.W., 2015. Simulação do processo de purificação do ácido láctico em um sistema de destilação reativa, in: Blucher Chemical Engineering Proceedings. Presented at the XX Congresso Brasileiro de Engenharia Química, pp. 12729–12735.
28. Kumar, R., Nanavati, H., Noronha, S.B., Mahajani, S.M., 2006. A continuous process for the recovery of lactic acid by reactive distillation. J. Chem. Technol. Biotechnol. 81, 1767–1777. https://doi.org/10.1002/jctb.1603

29. Laube, H., Matysik, F.-M., Schmidberger, A., Mehlmann, K., Toursel, A., Boden, J., 2016. CE-UV/VIS and CE-MS for monitoring organic impurities during the downstream processing of fermentative-produced lactic acid from second-generation renewable feedstocks. J. Biol. Eng. 10. https://doi.org/10.1186/s13036-016-0027-2
30. Li, G., Wang, C., Guang, C., Zhang, Z., 2020. Energy-saving investigation of hybrid reactive distillation for n-butyl acetate production from two blending feedstocks. Sep. Purif. Technol. 235, 116163. https://doi.org/10.1016/j.seppur.2019.116163
31. Li, Q., Kiss, A.A., 2021. Novel pervaporation-assisted pressure swing reactive distillation process for intensified synthesis of dimethyl carbonate. Chem. Eng. Process. - Process Intensif. 108358. https://doi.org/10.1016/j.cep.2021.108358
32. López-Garzón, C.S., Straathof, A.J.J., 2014. Recovery of carboxylic acids produced by fermentation. Biotechnol. Adv. 32, 873–904. https://doi.org/10.1016/j.biotechadv.2014.04.002
33. Luyben, W.L., 2013. Distillation design and control using Aspen simulation, 2nd ed. ed. Wiley, Hoboken, N.J.
34. Mizrahi, J., Eyal, A., Riki, C., Hazan, B., Starr, J.N., 2006. Process for producing a purified lactic acid solution. US7026145B2.
35. Moulijn, J.A., Stanckiewicz, A., 2017. Reactive Separations, in: Abraham, M.A. (Ed.), Encyclopedia of Sustainable Technologies. Elsevier, Oxford, pp. 565–572. https://doi.org/10.1016/B978-0-12-409548-9.10247-7
36. Mueller, I., Pech, C., Bhatia, D., Kenig, E.Y., 2007. Rate-based analysis of reactive distillation sequences with different degrees of integration. Chem. Eng. Sci., 8th International Conference on Gas-Liquid and Gas-Liquid-Solid Reactor Engineering 62, 7327–7335. https://doi.org/10.1016/j.ces.2007.08.044
37. Murphy, T., Blanch, H., Wilke, C., 1982. Water recycling in extractive fermentation. Process Biochem. 17, 6–40.
38. Musashino, 2020. Lactic Acid (50%, 88%, 90%) Manufacturer and seller | Musashino Chemical Laboratory | 50-21-5/598-82-3 | [WWW Document]. URL https://www.musashino.com/english/product/name/musashino_lactate/ (accessed 9.22.20).
39. Novita, F.J., Lee, H.-Y., Lee, M., 2018. Plantwide design for high-purity formic acid reactive distillation process with dividing wall column and external heat integration arrangements. Korean J. Chem. Eng. 35, 926–940. https://doi.org/10.1007/s11814-017-0342-4
40. Okano, K., Tanaka, T., Kondo, A., 2014. Lactic Acid, in: Bioprocessing of Renewable Resources to Commodity Bioproducts. John Wiley & Sons, Ltd, pp. 353–380. https://doi.org/10.1002/9781118845394.ch13
41. Oliveira, R.A.D., Alexandri, M., Komesu, A., Venus, J., Rossell, C.E.V., Filho, R.M., 2019. Current Advances in Separation and Purification of Second-Generation Lactic Acid. Sep. Purif. Rev. 0, 1–17. https://doi.org/10.1080/15422119.2019.1590412
42. Orjuela, A., Kolah, A., Lira, C.T., Miller, D.J., 2011. Mixed Succinic Acid/Acetic Acid Esterification with Ethanol by Reactive Distillation. Ind. Eng. Chem. Res. 50, 9209–9220. https://doi.org/10.1021/ie200133w
43. Orjuela, A., Santaella, M.A., Molano, P.A., 2016. Process Intensification by Reactive Distillation, in: Segovia-Hernández, J.G., Bonilla-Petriciolet, A. (Eds.), Process Intensification in Chemical Engineering: Design Optimization and Control. Springer International Publishing, Cham, pp. 131–181. https://doi.org/10.1007/978-3-319-28392-0_6

44. Quaglia, A., Pennati, A., Bogataj, M., Kravanja, Z., Sin, G., Gani, R., 2014. Industrial Process Water Treatment and Reuse: A Framework for Synthesis and Design. Ind. Eng. Chem. Res. 53, 5160–5171. https://doi.org/10.1021/ie401379j
45. Qureshi, Mohd.S., Bhongale, S.S., Thorave, A.K., 2011. Determination of organic acid impurities in lactic acid obtained by fermentation of sugarcane juice. J. Chromatogr. A 1218, 7147–7157. https://doi.org/10.1016/j.chroma.2011.08.025
46. ReportLinker, 2020. Global Lactic Acid Industry [WWW Document]. GlobeNewswire News Room. URL http://www.globenewswire.com/news-release/2020/07/17/2063773/0/en/Global-Lactic-Acid-Industry.html (accessed 12.14.20).
47. Sanz, M.T., Murga, R., Beltrán, S., Cabezas, J.L., Coca, J., 2004. Kinetic Study for the Reactive System of Lactic Acid Esterification with Methanol: Methyl Lactate Hydrolysis Reaction. Ind. Eng. Chem. Res. 43, 2049–2053. https://doi.org/10.1021/ie034031p
48. Schwarz, J., Beloff, B.R., Beaver, E.R., 2002. Use Sustainability Metrics to Guide Decision-Making. Chem. Eng. Prog. 98, 58–63.
49. Seider, W.D., 2017. Product and process design principles: synthesis, analysis, and evaluation, Fourth edition, EMEA edition. ed. John Wiley & Sons Inc, New York.
50. Seqens, 2021. Dimethyl Succinate [WWW Document]. Seqens. URL https://www.seqens.com/en/products/dimethyl-succinate/ (accessed 1.7.21).
51. Sheldon, R.A., 2018. Metrics of Green Chemistry and Sustainability: Past, Present, and Future. ACS Sustain. Chem. Eng. 6, 32–48. https://doi.org/10.1021/acssuschemeng.7b03505
52. Stankiewicz, A., Gerven, T.V., Stefanidis, G., 2019. The Fundamentals of Process Intensification. Wiley VCH.
53. Su, C.-Y., Yu, C.-C., Chien, I.-L., Ward, J.D., 2013. Plant-Wide Economic Comparison of Lactic Acid Recovery Processes by Reactive Distillation with Different Alcohols. Ind. Eng. Chem. Res. 52, 11070–11083. https://doi.org/10.1021/ie303192x
54. Sundmacher, K., Kienle, A. (Eds.), 2003. Reactive Distillation: Status and Future Directions. Wiley VCH, Weinheim.
55. Triantafyllou, C., Smith, R., 1992. The design and optimisation of fully thermally coupled distillation columns: Process design. Chem. Eng. Res. Des. https://doi.org/null
56. Uono, T., 2013. Processo de purificação do ácido láctico para sìntese do lactato. BRPI1003073A2.
57. Wang, C., Zhang, Z., Zhang, X., Gao, J., Stewart, B., 2019. Energy-saving hybrid processes combining pressure-swing reactive distillation and pervaporation membrane for n-propyl acetate production. Sep. Purif. Technol. 221, 1–11. https://doi.org/10.1016/j.seppur.2019.03.074
58. Weinfeld, J.A., Owens, S.A., Eldridge, R.B., 2018. Reactive dividing wall columns: A comprehensive review. Chem. Eng. Process. - Process Intensif. 123, 20–33. https://doi.org/10.1016/j.cep.2017.10.019
59. Yildirim, Ö., Kiss, A.A., Kenig, E.Y., 2011. Dividing wall columns in chemical process industry: A review on current activities. Sep. Purif. Technol. 80, 403–417. https://doi.org/10.1016/j.seppur.2011.05.009
60. Zhang, Y., Ma, L., Yang, J., 2004. Kinetics of esterification of lactic acid with ethanol catalyzed by cation-exchange resins. React. Funct. Polym. 61, 101–114. https://doi.org/10.1016/j.reactfunctpolym.2004.04.003

Tables

Table 1. Kinetic models and parameters for the five reactions included in this study

Eq.	Reaction rate expression	Reaction type	Pre-exponential factor ($kmol/kg_{cat} \cdot s$)	Activation energy (kJ/kmol)
1	$r = m_{cat}\left(k_f a_{LA} a_{MOH} - k_r a_{ML} a_{water}\right)$	LA esterification to ML	2.17e+04	48,733
		ML hydrolysis to LA	1.06e+03	48,487
2	$r = m_{cat}\left(k_f x_{SA} x_{MOH} - k_r x_{MMS} x_{water}\right)$	SA esterification to MMS	1.10e+07	72,855
		MMS hydrolysis to SA	2.45e+05	72,855
3	$r = m_{cat}\left(k_f x_{MMS} x_{MOH} - k_r x_{DMS} x_{water}\right)$	MMS esterification to DMS	4.40e+07	78,646
		DMS hydrolysis to MMS	5.57e+06	78,646
4	$r = m_{cat}\left(k_f x_{LA}^2 - k_r x_{Di-LA} x_{water}\right)$	LA oligomerisation to Di-LA	2.00e+01	52,000
		Di-LA desoligo-merisation to LA	9.99e+01	52,000
5	$r = m_{cat}\left(k_f x_{LA} x_{Di-LA} - k_r x_{Tri-LA} x_{water}\right)$	Di-LA oligomeri-sation to Tri-LA	5.70e+00	50,800
		Tri-LA desoligo-merisation to Di-LA	2.85e+01	50,800

r: rate of reaction (kmol/s), m_{cat}: catalyst mass (kg_{cat}), k_f: forward rate of reaction constant ($kmol/kg_{cat}*s$), k_r: reverse rate of reaction constant ($kmol/kg_{cat}*s$), a_i: activity, x_i: mole fraction

Table 2. Boiling temperatures of pure components and azeotropes at different pressures

Component Azeotrope*	0.1 atm		0.5 atm		1.0 atm		Decomposition temperature (°C)
	Boiling point (°C)	Azeotrope composition (mol frac)	Boiling point (°C)	Azeotrope composition (mol frac)	Boiling point (°C)	Azeotrope composition (mol frac)	
MeOH	15.7	-	47.9	-	64.5	-	-
Water/DMS	45.7	0.96/0.4	80.8	0.95/0.05	98.9	0.95/0.05	-
ML/water	46.0	0.02/0.98	81.4	0.04/0.96	99.6 99-99.5***	0.05/0.95 0.05/0.95***	-
Water	46.1	-	81.7	-	100.0	-	-
ML	81.9	-	123.2	-	144.8	-	385**
LA/DMS	125.1	0.04/0.96	169.9	0.17/0.83	192.8	0.23/0.77	-
Di-LA/DMS	124.9	0.06/0.94	170.1	0.13/0.87	193.6	0.17/0.83	-
DMS/MMS	-	-		-	-	-	-
DMS	125.2	-	171.6	-	196.4	-	365**
Di-LA	150.6	-	193.7	-	215.9		-
LA/Di-LA/MMS	-	-		-	216.4	0.82/0.04/0.14	-
LA/MMS	154.6	0.48/0.52	195.5	0.73/0.27	216.4	0.83/0.17	-
LA	156.5	-	196.2	-	216.6	-	300
MMS	165.1	-	200.0	-	222.9	-	-
SA	244.5	-	292.5	-	317.6	-	235
Tri-LA	272.3	-	320.9	-	345.9	-	-

*All azeotropes are homogeneous

**Autoignition temperature

*** Experimental data (Chahal, 2000)

1 **Table 3.** Setup parameters and key results tracked to simulate a dual R-DWC

Description	Units	Base Case	Fully thermally coupled	Fully thermally + recycle
Setup parameters esterification column				
Number of stages		29	25	25
Specified bottoms to feed ratio		0.020	0.015	0.015
Number of rectification stages		4	8	8
Number of reactive stages		20	12	12
Number of stripping stages		5	5	5
Catalyst mass per stage	kg	10.0	10.0	10.0
Feed lactic acid stage		3	6	6
Feed methanol stage		24	20	20
Setup parameters hydrolysis column				
Number of stages		85	85	85
Specified bottoms rate	kmol/h	6.2	6.6	6.6
Specified boilup ratio		5.5	5.5	5.5
Number of rectification stages		20	10	10
Number of reactive stages		45	30	30
Number of stripping stages		20	45	45
Catalyst mass per stage	kg	16	12, 14	12, 14
Methanol makeup flowrate*	kmol/h	4.828	9.295	0.813
Results esterification column				
Equipment related results				
Temperature top stage	°C	85.6	83.0	83.0
Temperature bottom stage	°C	178.9	182.2	183.1
Reboiler duty	kW	344.7	432.6	426.6
Stream results				
Preconcentrated LA (Feed to C1)	kmol/h	19.269	22.654	22.654
LA	kmol/h	4.140	4.152	4.152
Water	kmol/h	14.598	17.971	17.971
Vapour stream from C1	kmol/h	30.521	38.397	38.514
MeOH	kmol/h	4.245	8.696	8.778
Water	kmol/h	21.768	25.239	25.276
ML	kmol/h	4.507	4.461	4.459
Liquid returning stream to top of C1	kmol/h	2.780	2.780	2.780
MeOH	kmol/h	0.116	0.118	0.119
Water	kmol/h	2.236	2.332	2.332
ML	kmol/h	0.428	0.250	0.250
Impurities from C1	kmol/h	0.566	0.542	0.544
Di-LA	kmol/h	0.026	0.008	0.008
SA	kmol/h	0.061	0.124	0.128
MMS	kmol/h	0.289	0.239	0.224
DMS	kmol/h	0.180	0.168	0.179
Intermediate esterification targets				
ML top split fraction		1.000	1.000	1.000
DMS bottom split fraction		0.999	1.000	1.000
LA conversion	%	99.77	99.93	99.88
LA lost in C1	%	1.48	0.48	0.53
Impurities molar fraction (DMS+MMS+SA)	mol fr	0.94	0.98	0.98
Results hydrolysis column				
Equipment related results				
Temperature top stage	°C	59.5	57.6	57.6
Temperature bottom stage	°C	101.8	106.9	106.9

Condenser duty	kW	635.2	888.1	889.3
Reboiler duty	kW	280.5	447.8	447.8
Reflux ratio	molar	1.671	1.703	1.696
Stream results				
Vapour stream from C1 (Feed to C2)	kmol/h	30.521	38.397	38.514
MeOH	kmol/h	4.245	8.696	8.778
Water	kmol/h	21.768	25.239	25.276
ML	kmol/h	4.507	4.461	4.459
Side-draw from C2	kmol/h	2.780	2.780	2.780
MeOH	kmol/h	0.116	0.118	0.119
Water	kmol/h	2.236	2.332	2.332
ML	kmol/h	0.428	0.250	0.250
LA product	kmol/h	6.960	6.618	6.618
LA	kmol/h	3.601	4.003	4.001
Di-LA	kmol/h	0.013	0.009	0.009
Water	kmol/h	3.249	2.578	2.579
ML	kmol/h	0.096	0.028	0.028
Excess MeOH and water from C2	kmol/h	20.781	28.999	29.116
MeOH	kmol/h	7.758	12.679	12.758
Water	kmol/h	12.668	16.237	16.275
ML	kmol/h	0.355	0.082	0.082
Intermediate hydrolysis targets				
Methyl lactate conversion	%	88.94	97.38	97.38
LA lost as ML (top)	%	8.57	1.98	1.98
LA lost as ML (bottom)	%	2.32	0.68	0.68
Final targets				
LA product	kg/h	395.120	411.463	411.329
LA+Di-LA	wt fr	0.826	0.880	0.880
Water	wt fr	0.148	0.113	0.113
ML	wt fr	0.025	0.007	0.007
Purification section LA recovery	%	86.98	96.41	96.37
Overall LA recovery	%	86.11	95.72	95.67

*Defined by the design specification over the temperature in the reactive section

Table 4. Process comparison in terms of key performance indicators

	Parameter description	Su et al. (2013)	Kim et al. (2017)	This work
Mass balance key streams and parameters	Feed to preconcentration (kg/h)	1255.1	1255.1	1255.2
	LA to preconcentration (kg/h)	376.5	376.5	376.6
	MeOH makeup (kg/h)	6.4	6.4	26.1*
	MeOH recycled (kg/h)	311.0	310.5	406.4
	Feed to purification (kg/h)	592.4	592.8	760.5
	LA to purification (kg/h)	376.0	376.4	374.0
	Water for the hydrolysis section (kg/h)	252.2	252.2	0.0
	Impurities removed (kg/h)	67.2	67.6	73.3
	LA product (kg/h)	413.5	420.4	411.3
	Plant capacity (ktpy)	3.5	3.5	3.5
	MeOH/feed molar ratio	1.6	1.7	0.6
	MeOH/LA feed molar ratio	4.0	4.0	3.3
	LA recovery (%)	91.8	94.2	95.7
	CO_2 emission rate (kg CO_2/h)	417	349	280
Energy used	Heating duty (kW)	1763	1474	1280
	Cooling duty (kW)	1687	1388	1177
Sustainability metrics	Material intensity (kg_{input}/kg LA)	0.379	0.357	0.256
	E-factor (kg_{waste}/kg LA)	0.163	0.161	0.178**
	Energy intensity (MJ/kg LA)	15.3	12.6	11.2
	Water consumption (m^3/kg LA)	0.052	0.043	0.033
	CO_2 emissions (kg CO_2/kg LA)	1.01	0.83	0.68

* Additional makeup required due to side reactions

**Higher waste production due to side reactions

Figure captions (auto-updated)

Figure 1. Process block diagram for conventional LA production. The dotted block includes the steps evaluated in this study (modified from (Alves de Oliveira et al., 2018; López-Garzón and Straathof, 2014)

Figure 2. Sections and interconnections from the decomposition approach. The dotted and dashed boxes indicate the system boundaries for the shortcut calculations.

Figure 3. Methodology to implement a rigorous simulation of a fully-thermally coupled arrangement with two reactive sections (dashed connections considered after first iteration, yellow: initialisation values adjustment, green: esterification column implementation, red: hydrolysis column implementation, blue: coupling)

Figure 4. Production rate of the esterification products a) At different temperatures b) At different pressures at the boiling temperature of ML

Figure 5. Sensitivity analysis of the effect of the heater outlet temperature in the preconcentration arrangement (The dotted line indicates the maximum LA loss allowed)

Figure 6. Column profiles for the esterification section (*stoichiometric ratio)

Figure 7. Sensitivity analysis of the effect of liquid split ratio on the esterification section

Figure 8. Column profiles for the hydrolysis column with the shaded region representing the reactive section (*mass of catalyst per stage in kg)

Figure 9. Process flowsheet and key stream data for the preconcentration and purification of LA. The dashed box presents the fully-thermally coupled arrangement equivalent to a dual R-DWC (◊ stream number, □ inlet stage, ○ total number of stages, ▭ stages per section, B/F bottom-to-feed molar ratio, RR reflux ratio, LS liquid split ratio)

Figure 10. Composite curves of the process

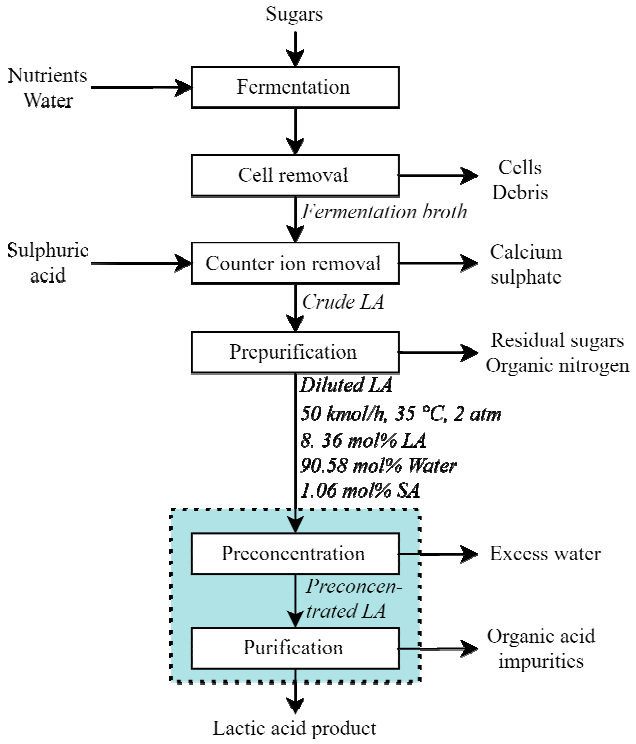

Figure 1. Process block diagram for conventional LA production. The dotted block includes the steps evaluated in this study (modified from (Alves de Oliveira et al., 2018; López-Garzón and Straathof, 2014)

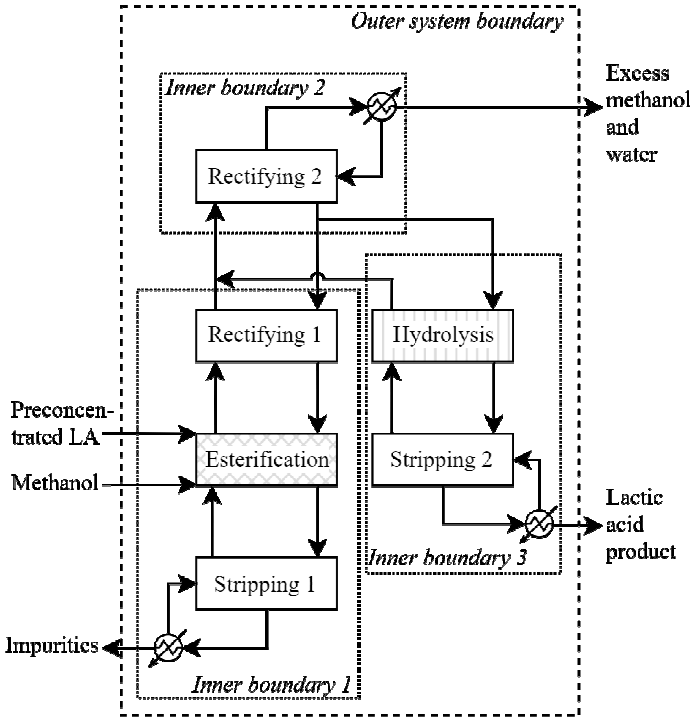

Figure 2. Sections and interconnections from the decomposition approach. The dotted and dashed boxes indicate the system boundaries for the shortcut calculations.

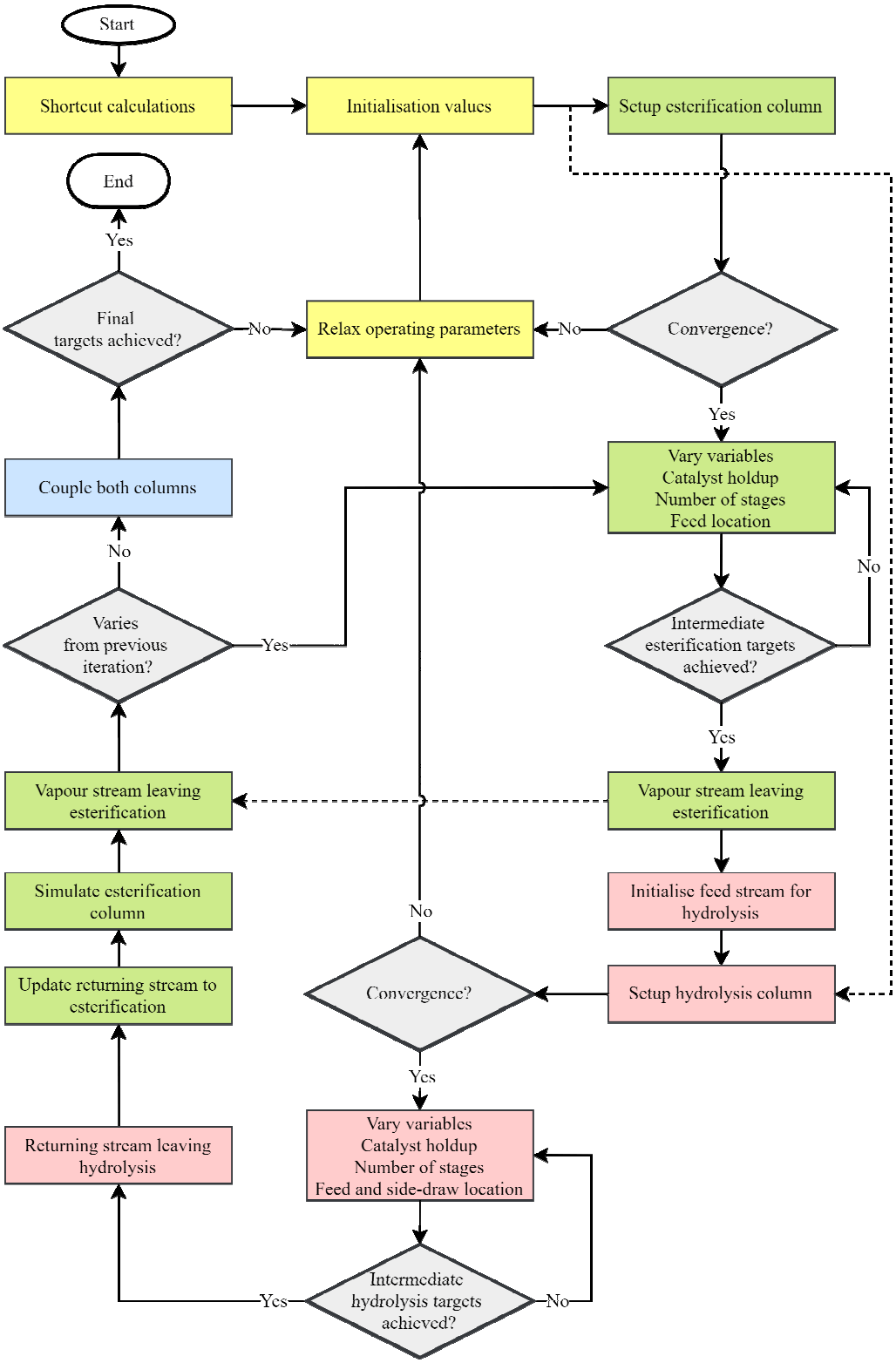

Figure 3. Methodology to implement a rigorous simulation of a fully-thermally coupled arrangement with two reactive sections (dashed connections considered after first iteration, yellow: initialisation values adjustment, green: esterification column implementation, red: hydrolysis column implementation, blue: coupling)

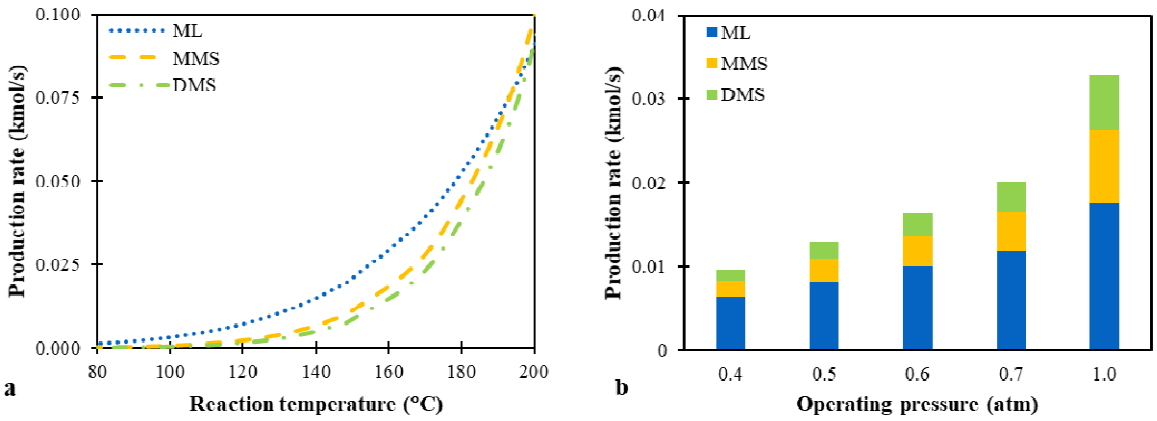

Figure 4. Production rate of the esterification products a) At different temperatures b) At different pressures at the boiling temperature of ML

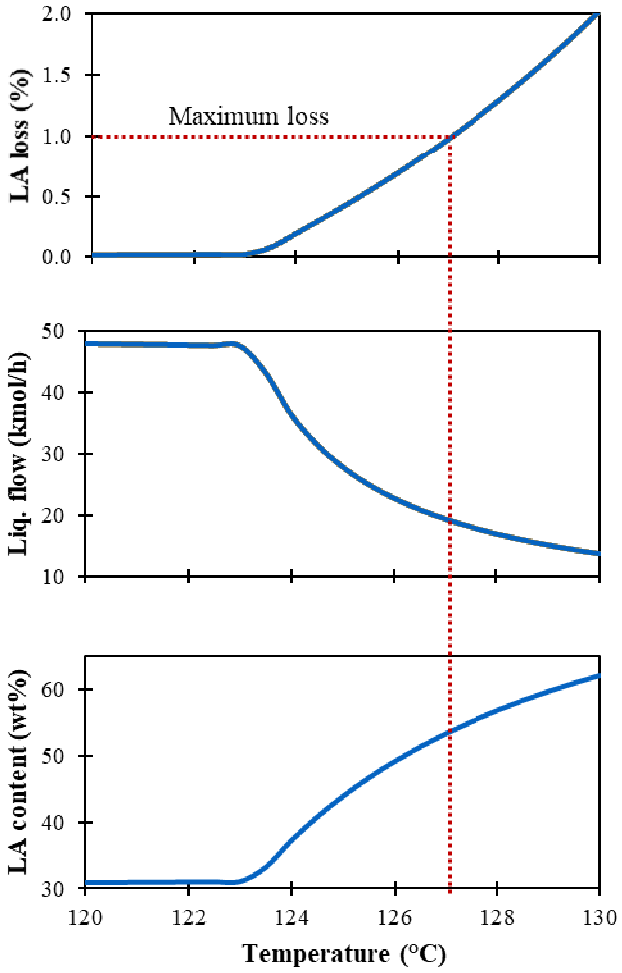

Figure 5. Sensitivity analysis of the effect of the heater outlet temperature in the preconcentration arrangement (The dotted line indicates the maximum LA loss allowed)

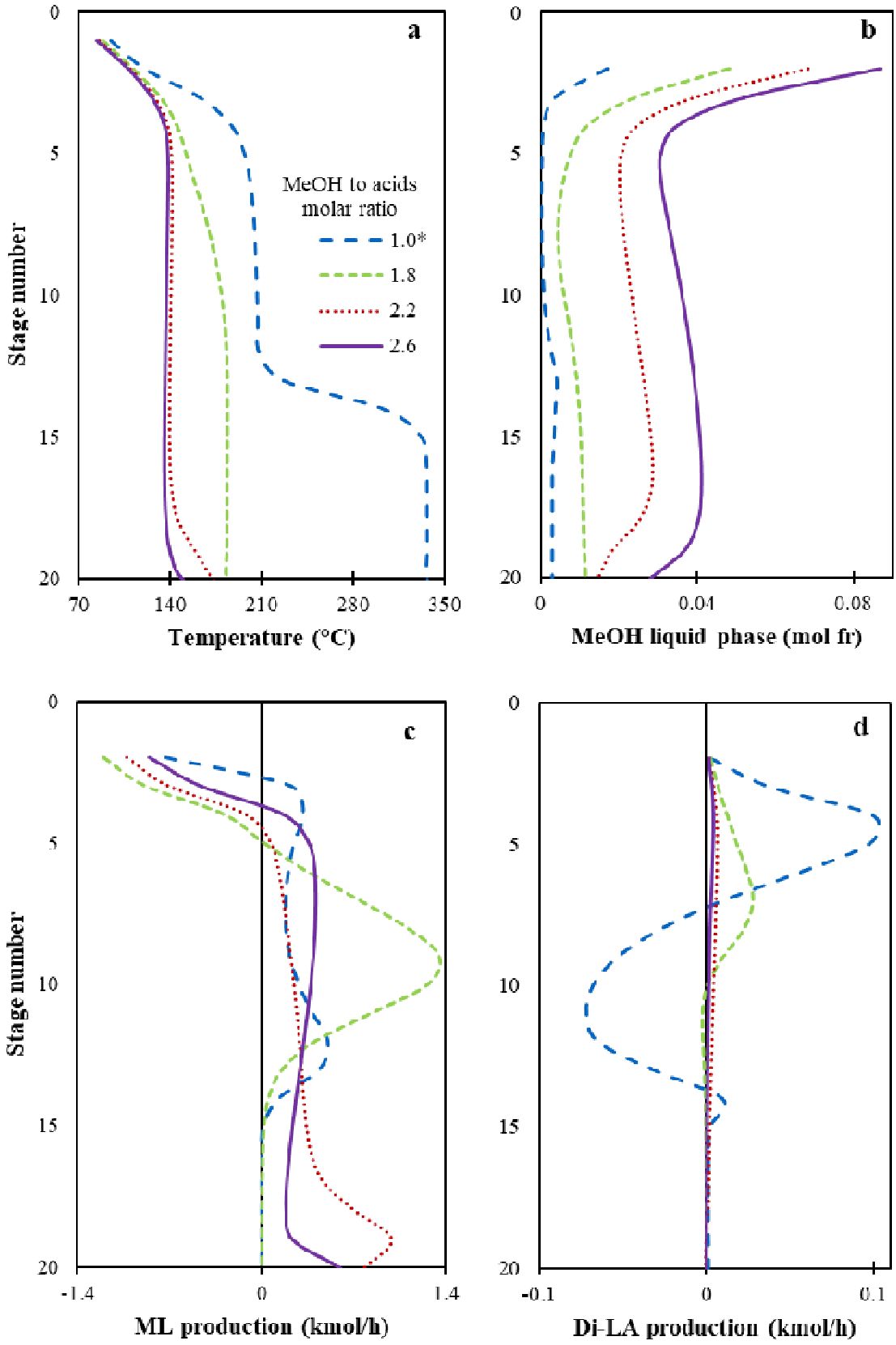

Figure 6. Column profiles for the esterification section (*stoichiometric ratio)

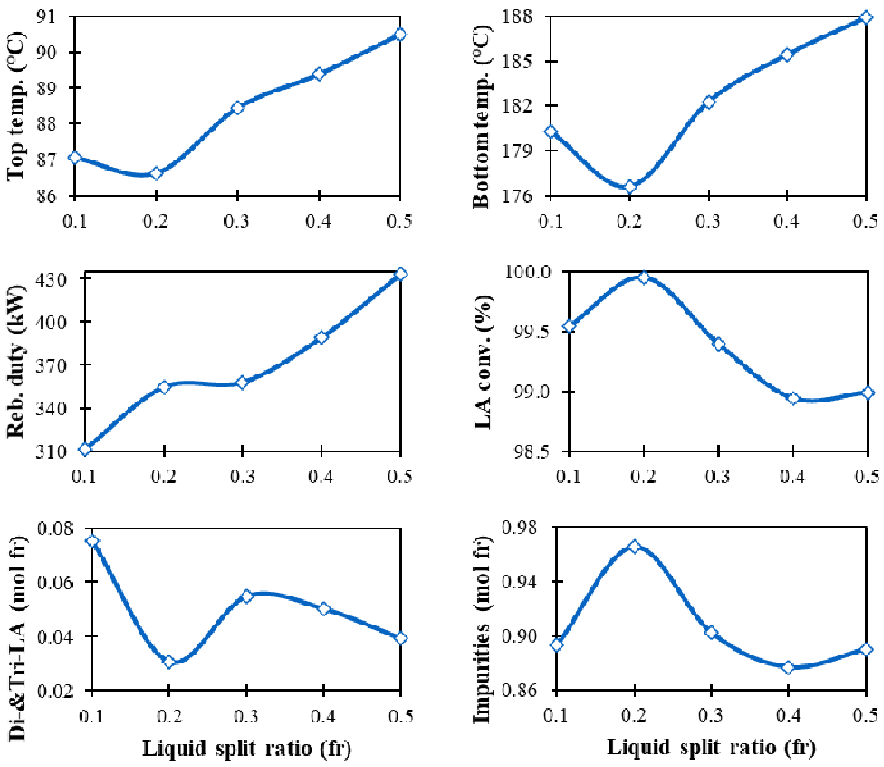

Figure 7. Sensitivity analysis of the effect of liquid split ratio on the esterification section

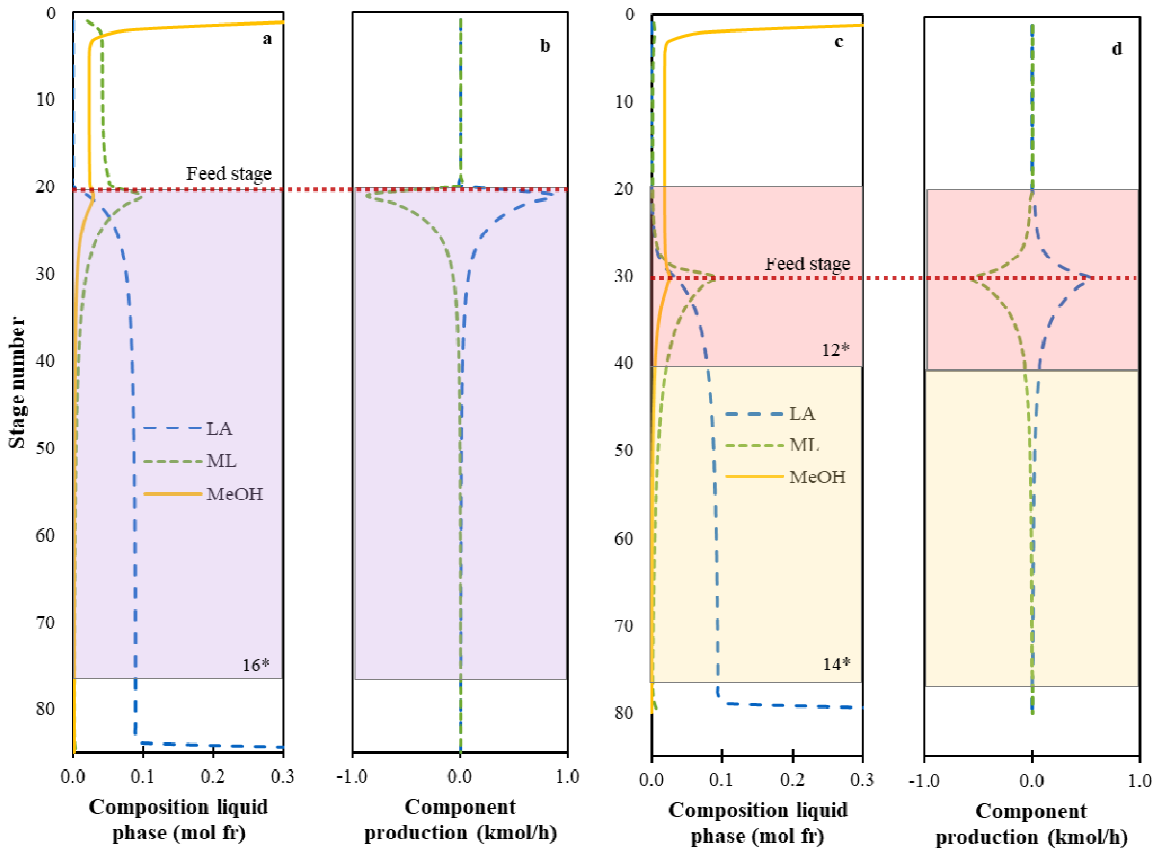

Figure 8. Column profiles for the hydrolysis column with the shaded region representing the reactive section (*mass of catalyst per stage in kg)

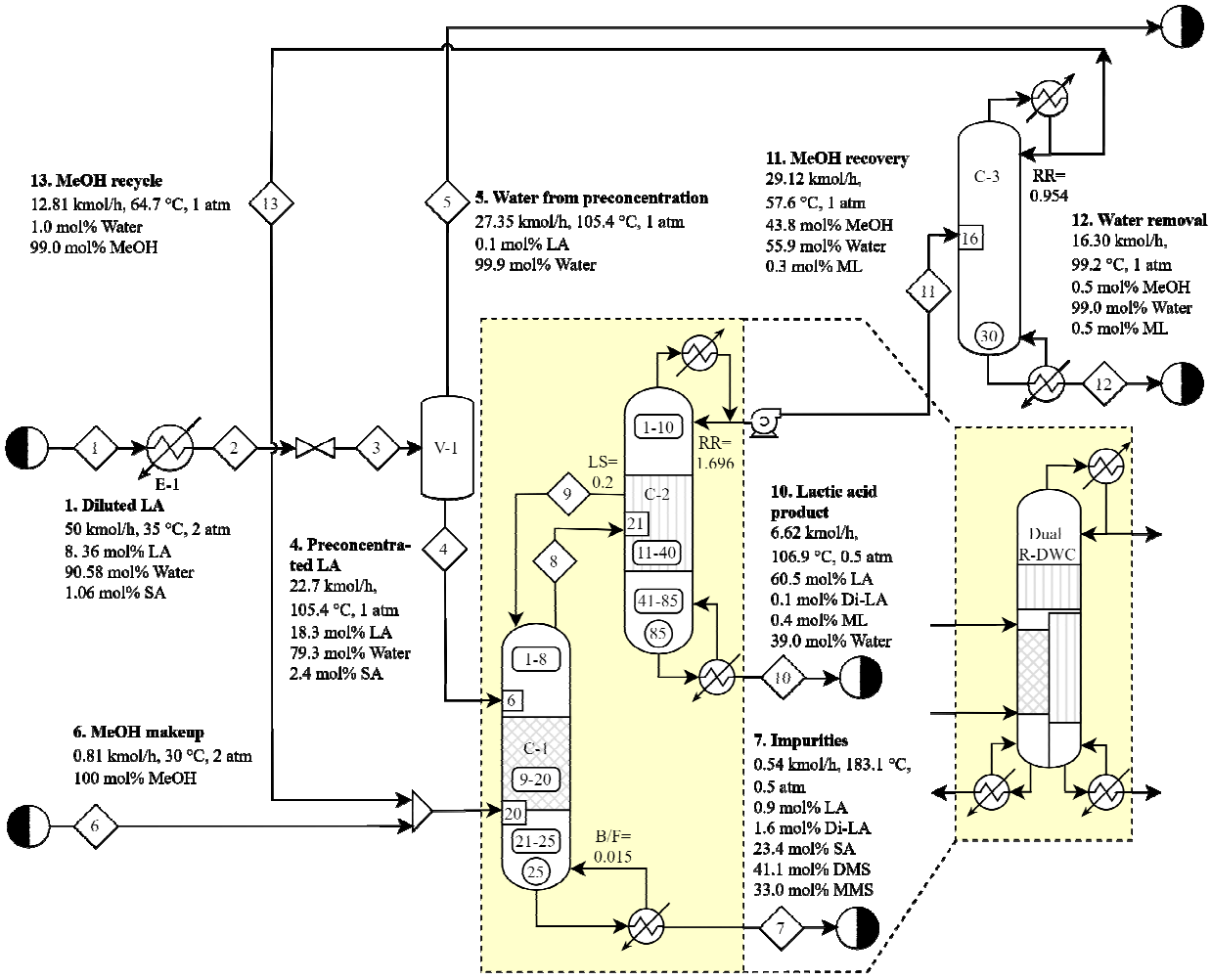

Figure 9. Process flowsheet and key stream data for the preconcentration and purification of LA. The dashed box presents the fully-thermally coupled arrangement equivalent to a dual R-DWC (◊ stream number, □ inlet stage, ○ total number of stages, ▭ stages per section, B/F bottom-to-feed molar ratio, RR reflux ratio, LS liquid split ratio)

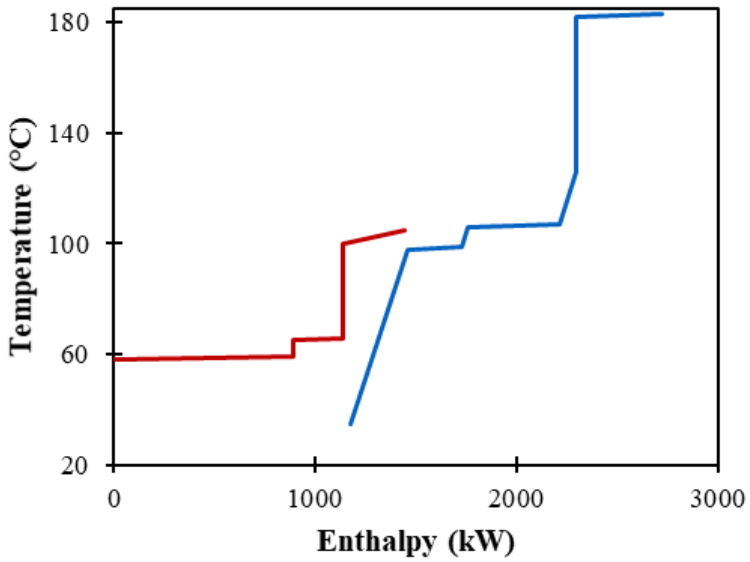

Figure 10. Composite curves of the process

Supplementary information

Conceptual design of a dual reactive dividing wall column for downstream processing of lactic acid

Isabel Pazmiño-Mayorga, Megan Jobson, Anton A. Kiss

Department of Chemical Engineering and Analytical Science, The University of Manchester, Sackville Street, Manchester, M13 9PL, United Kingdom

The Supplementary information presents a comprehensive reference for the calculations and setup parameters used to implement a dual-reactive dividing wall column in Aspen Plus and the corresponding results.

Nomenclature

LA: lactic acid

MeOH: methanol

EtOH: ethanol

ML: methyl lactate

MMS: monomethyl succinate

MES: monoethyl succinate

DMS: dimethyl succinate

1. Phase equilibrium data

1.1 Validation of the thermodynamic model

The first validation was performed over the MeOH-ML pair with the experimental data from Sanz et al. (2002), which offered molar liquid and vapour fractions at 33.33, 66.66, and 101.33 kPa. Figure S1 depicts the experimental data points and the prediction obtained from Aspen Plus, and there is a good fit.

In contrast to the SA-MeOH system, the SA-EtOH system has been widely studied, and more kinetic, and VLE data is available (Altuntepe et al., 2017; Orjuela et al., 2011). Therefore, VLE data about water-MES was used to validate the water-MMS' predicted values, where the differences in behaviour are expected to be non-significant. The work of Orjuela et al. (2011) provided the VLE data for the water-MES system at 323.15 K. Figure S2 presents the experimental data points and the predictions from Aspen Plus, and there is a good fit. As a result, the estimated binary parameters were used to build the simulation.

2. Research approach

2.1 Detailed description of the decomposition approach applied to a dual reactive system

The decomposition approach, now applied to a system that includes two reactions, requires several iterations to find an adequate configuration. Once the required tasks have been identified, the inlet, outlet and internal flows needed to be located to achieve the removal, enrichment or transformation required. Thus, the preconcentrated LA and the MeOH stream were fed to the esterification column at the top and bottom of the reactive zone, respectively. The ML-rich vapour stream moved upwards to the rectifying section 1 together with the lighter products. The rectifying section 1 is expected to be small, as the main objective of the liquid stream returning to the esterification section is to maintain the downward flow of liquid, so a sharp separation is not required. The stripping section 1, below the esterification section, is meant to remove DMS and heavier components.

The vapour stream leaving the rectifying section 1 contained ML, the water necessary for the hydrolysis reaction, and the excess MeOH to be recovered and recycled. Thus, this stream

was initially directed to the rectifying section 2, where MeOH and the excess water will flow upwards while ML and water were directed to the hydrolysis section to react. Then, the vapour stream leaving the hydrolysis section, rich in the light products of the reaction (MeOH), was directed to the rectifying section 2 to remove the lightest component and the unreacted and excess water from the system.

The liquid stream leaving the rectifying section 2 is split into two streams, one returning to the rectifying section 1 and the other to the hydrolysis section, defined by the liquid split ratio. The liquid stream leaving the hydrolysis section entered the stripping section 2 to guarantee the product's specification by pushing upwards and maintaining the ML inside the reactive zone.

The decomposition approach for the design of a DWC (Triantafyllou and Smith, 1992) and the extension for the design of an R-DWC with the reactive section in the feed side of the wall (Mueller et al., 2007) used the vapour-liquid equilibrium data to obtain the composition of the returning stream to the column on the feed side of the wall, using either a total or partial condenser. However, the configuration proposed in this work contained two reactive sections, one at each side of the wall. Therefore, the composition of the returning stream would depend not only on the separation accomplished due to the vapour-liquid equilibrium but also on the rate of consumption and production of components on the second reactive section, which is further explored when coupling both sections.

2.2 Detailed description of the shortcut calculations

Once the tasks and interconnections were placed, different system boundaries were defined to carry out mass balances. The outer system boundary contained all sections to target the top stream's compositions containing MeOH and water and the concentrated LA product stream on specification. For the inner boundary 1, full conversion of LA and SA with a stoichiometric feed of MeOH was assumed to start the calculations to update the impurities stream's flowrate and composition, which was assumed to contain only DMS. The returning stream was initially set to zero as iterative calculations are required that depend on the split ratio of the liquid stream leaving the rectifying section 2. Then, the vapour stream's flowrate and composition, leaving the inner boundary 1, were defined and used for the next calculation.

For the inner boundary 2, two streams are known, the product stream and the vapour inlet stream; while the others required initialisation, the vapour and liquid streams leaving and entering the hydrolysis section. The liquid stream entering the hydrolysis section depends on

the liquid split ratio above the wall, defined as the molar flowrate returning to the esterification section over molar flowrate towards the hydrolysis section. As the objective is to drive LA production in the hydrolysis section, most ML needs to be driven to this section, whereas avoiding drying out the upper trays in the rectifying section 1. Therefore, a liquid split ratio of 0.1 to 0.5 towards the esterification section was systematically tested by varying it with steps of 0.1. The bottom to feed molar ratio in the inner boundary 1 was calculated and updated accordingly. The new values for the stream leaving the esterification section were used to update the balance in the inner boundary 2.

2.3 Detailed description of the rigorous simulation of a dual-reactive dividing wall column and the recovery column at a flowsheet level

The esterification section, rectifying section 1 and stripping section 1 were implemented in a RadFrac module. The initial set up parameters included a reboiler, a total condenser and a relatively large number of stages for each section (e.g., 30). The operating pressure was selected after evaluating the boiling points and the required split, and the pressure drop was neglected at this stage of the design. The five equilibrium reactions were implemented using the built-in power law, setting the type of reaction as kinetic and defining a liquid reacting phase. The holdup in the reactive zone was specified as the mass of catalyst, as required by the kinetic equation. A mass holdup of 10 kg per stage, used in Su et al. (2013), was employed to initialise the simulation. Structured packing was selected because of the operating pressure (mild vacuum) and the low liquid rates, in addition to the advantages of packing over trays for small-columns to reduce the pressure drop and improve the separation efficiency (Pilling and Holden, 2009). The packing selected was MellapakPlus 252Y, due to its high capacity, with an HETP of 0.4 m. At the moment, Aspen Plus does not provide options for structured packing tailored for reactive distillation, such as Katapak-SP, which consists of a flexible design combining catalyst elements and MellapakPlus layers (i.e., solid catalyst included in packing) (Sulzer Chemtech, 2013). However, the similarity on the hydraulic behaviour is expected to provide an accurate estimation of the column diameter, determined with the packing sizing tool in Aspen Plus. The F-factors for the esterification and hydrolysis sections of the column range between 1.37-2.44 $Pa^{0.5}$ and 1.34-3.19 $Pa^{0.5}$, respectively. According to the data from the vendor (Sulzer), these values correspond to pressure drops of 0.4-1.5 mbar/m and 0.4-2 mbar/m which is practically negligible. Therefore, assuming no pressure drop across the column for the simulation does not present significant changes to the material and energy balances. However, care should be taken when using

internals that have a higher pressure drop per stage as the impact could be more significant. The number of stages in each section required fine-tuning to guarantee that enough reactive stages and catalyst holdup are available to achieve a high conversion (> 99 %) and that the desired separation is achieved (Al□Arfaj and Luyben, 2000). The bottom to feed molar ratio and the reflux ratio obtained from the shortcut calculations were used to setup the operating parameters.

The preconcentrated LA stream was initially fed in the first reactive stage, and the MeOH stream was located in the last reactive stage. As MeOH will be recovered and recycled, a mixing point was included to consider the recycling stream and the makeup. The stream representing the recycle was initialised with a MeOH flowrate in a stoichiometric ratio. The makeup stream is initialised with a low flowrate, for example, 0.01 kmol/h and adjusted after the sensitivity analysis. The logic behind selecting the MeOH flowrate (and not the MeOH to feed ratio) to maintain the reactive zone's temperature was based on the control loops usually used for reactive distillation and by taking into account inaccuracies of flow measurements and changes in composition (Luyben, 2013). The MeOH flowrate resulted from a design specification to maintain the last reactive stage temperature at 145±2 °C while varying the MeOH makeup stream flowrate. As the implementation of a thermally coupled arrangement required removing the condenser and placing a returning liquid stream, the makeup stream required adjustment. The composition and flowrate of the returning liquid stream required iterative calculations because of the separation and reaction's simultaneous occurrence. The liquid split ratio was defined in a sensitivity analysis. Convergence issues appeared during the simulation, so the operating parameters were relaxed around the initialisation values obtained from the shortcut calculations.

The hydrolysis section, rectifying section 2 and stripping section 2 were implemented in a RadFrac module, which was initially not coupled to the previous column. The initial setup included a reboiler, a total condenser and a large number of stages per section following the procedure described for the esterification column. The operating parameters defined were the bottom rate and the reflux ratio, using the shortcut calculations' results. The reactions were setup in the same manner as the esterification column. The catalyst holdup was initialised with 10 kg per stage. The inlet vapour stream was specified using the simulation's values from the previous column's top outlet stream. The flowrate of the liquid side draw was specified based on the 0.2 liquid split ratio, obtained from the sensitivity analysis. The inlet stream was initially located in the top reactive stage. The liquid side draw was located on the stage above,

so that the composition is not much varied preparing the model for the thermal coupling (Smith, 2016).

The number of stages in each section, the catalyst holdup and the inlet stage were systematically varied to guarantee a high ML conversion and avoid losing ML in the top and bottom streams. That is, the number of reactive stages was increased in steps of two, and the catalyst holdup was increased in two kilograms per stage so that the conversion and the flowrate of ML improve. In the same manner, the location of the inlet stream and the side draw were varied to minimise the loss of ML from both ends of the column. The operating parameters were relaxed around the initialisation values as the separations obtained were not sharp, and the conversion is not total. Also, the boilup ratio was set as the operating parameter instead of the reflux ratio, as the former presented a larger influence over the bottom stream. These changes were monitored with the column profiles for temperature, the liquid phase composition in each stage and the production rates, and the results of the mass and energy balances. A sensitivity analysis of the operating parameters allowed finding a combination that to reach the product's target specifications while reducing the ML loss.

The coupling of both columns required several iterations that used the simulation results and updated values from the mass balances that account for non-sharp separations. Figure S3 describes the steps used to build the simulation in Aspen Plus. Specifically, the returning stream's composition was updated in the esterification column, which initially did not consider ML, as full conversion was assumed. Several iterations were performed by updating the vapour stream exiting the esterification column, and the liquid side-stream returning to the esterification column. Once the values did not change significantly, the esterification column's vapour stream replaced the hydrolysis column's temporary stream. Additional updating was performed until the returning stream's parameters did not change, so the connection was completed. The reconciliation feature for streams in Aspen Plus and estimates of temperature, flowrate and composition for the RadFrac modules were activated to facilitate the simulation's convergence. In this manner, a previously converged simulation's initial values are in place for a new run after a significant modification is performed. More powerful convergence methods may also be needed and tested if convergence issues appear.

From the esterification-hydrolysis arrangement simulation, the distillate stream's flowrate and composition were used in the shortcut model DSW to obtain initial parameters to set up a rigorous model of the MeOH recovery column. The column was specified with a reflux ratio of one. The recovery of the light key component, MeOH, was set to a value close to one. A total condenser and operation at one atmosphere with no pressure drop along the column were

initially set. A brief sensitivity analysis was performed to vary the reflux ratio and obtain the corresponding number of theoretical stages. The purity of the MeOH stream was specified as 99 % mol. The parameters of reflux ratio, number of stages, feed stage and distillate to feed ratio obtained from the shortcut model were used to implement the rigorous distillation column in a RadFrac module. By varying the reflux ratio, a design specification was set to achieve a composition of the distillate stream as 99 % mol MeOH and 1 % mol water, which then will be recycled to the esterification section.

The value of the recycle stream's flowrate was updated in the temporary stream located in the mixer prior the MeOH inlet to the esterification-hydrolysis unit, and the makeup value was adjusted manually to obtain a total MeOH feed equal to the previous converged simulation. Even though the makeup stream was adjusted with the design specification, setting an initial value closer to the "optima" value facilitated convergence. The adjustment was repeated until there was no change in the flowrate and composition of the recycle stream. The reconcile feature for streams was applied to the distillate stream from the recovery column, which was also declared as a tear stream. Finally, the recycle stream was connected, and the simulation was satisfactorily run and converged. These results demonstrated the model's robustness to operate with changing conditions and provided the mass and energy balances for evaluating the performance.

2.4 Heat integration

The stream data used for the heat integration is presented in Table S1. Table S2 presents the setup parameters for the utilities used in this study.

3. Results and discussion

3.1 Boiling point temperatures of pure components and azeotropes at different pressures

Table S3 presents an extended dataset of the boiling points of the pure compounds and the azeotropes in the system at different pressures, as part of the analysis to select the operating temperature.

3.2 Initialisation values for the rigorous simulation

Figure S4 presents a block diagram with the inlet, outlet and interconnecting streams, and Table S4 details the mass balance results obtained when defining a liquid split ratio of 0.4

3.3 Setup parameters and results for the sensitivity analysis over the liquid split ratio

Table **S5** indicates the setup parameters and the sensitivity analysis results where the liquid split ratio was changed from 0.1 to 0.5 in steps of 0.1.

3.4 Mass balance and performance indicators

Figure S5 presents the process flow diagram for the preconcentration and purification of LA. First, the diluted LA feed entered a flash vessel (V-1) arrangement, including a heater and a valve. The water-rich vapour stream left the system, while the liquid stream LA entered the esterification column (C-1). The impurities were removed in the bottom stream of C-1. The ML-rich stream was then fed to the reactive section in the hydrolysis column (C-2) while a liquid side-draw entered the top of C-1. The LA product was removed from the bottom of C-2. The distillate stream from C-2 entered a distillation column (C-3) to remove excess water and recover MeOH. Table S6 presents the flow summary for the flowsheet, and Table S7 presents the design features of the main vessels found to achieve the desired product.

4. References

1. Al-Arfaj, M.A., Luyben, W.L., 2000. Effect of number of fractionating trays on reactive distillation performance. AIChE J. 46, 2417–2425. https://doi.org/10.1002/aic.690461210
2. Altuntepe, E., Reinhardt, A., Brinkmann, J., Briesemann, T., Sadowski, G., Held, C., 2017. Phase Behavior of Binary Mixtures Containing Succinic Acid or Its Esters. J. Chem. Eng. Data 62, 1983–1993. https://doi.org/10.1021/acs.jced.7b00005
3. Luyben, W.L., 2013. Distillation design and control using Aspen simulation, 2nd ed. ed. Wiley, Hoboken, N.J.
4. Mueller, I., Pech, C., Bhatia, D., Kenig, E.Y., 2007. Rate-based analysis of reactive distillation sequences with different degrees of integration. Chem. Eng. Sci., 8th International Conference on Gas-Liquid and Gas-Liquid-Solid Reactor Engineering 62, 7327–7335. https://doi.org/10.1016/j.ces.2007.08.044
5. Orjuela, A., Yanez, A.J., Evans, J., Hassan, A.M., Miller, D.J., Lira, C.T., 2011. Phase equilibria in binary mixtures with monoethyl succinate. Fluid Phase Equilibria 309, 121–127. https://doi.org/10.1016/j.fluid.2011.06.020
6. Pilling, M., Holden, B.S., 2009. Choosing Trays and Packings for Distillation. Chem. Eng. Prog. 7.
7. Sanz, M.T., Calvo, B., Beltrán, S., Cabezas, J.L., 2002. Vapor−Liquid Equilibria at (33.33, 66.66, and 101.33) kPa and Densities at 298.15 K for the System Methanol + Methyl Lactate. J. Chem. Eng. Data 47, 1003–1006. https://doi.org/10.1021/je025513v
8. Smith, R., 2016. Chemical Process Design and Integration, 2nd edition. ed. Wiley-Blackwell, Chichester, West Sussex, United Kingdom.
9. Su, C.-Y., Yu, C.-C., Chien, I.-L., Ward, J.D., 2013. Plant-Wide Economic Comparison of Lactic Acid Recovery Processes by Reactive Distillation with

Different Alcohols. Ind. Eng. Chem. Res. 52, 11070–11083. https://doi.org/10.1021/ie303192x
10. Sulzer Chemtech, 2013. Structured Packings for Distillation, Absorption and Reactive distillation (Brochure). Sulzer Chemtech.
11. Triantafyllou, C., Smith, R., 1992. The design and optimisation of fully thermally coupled distillation columns: Process design. Chem. Eng. Res. Des. https://doi.org/null
12. Turton, R., 2018. Analysis, synthesis, and design of chemical processes, Fifth edition. ed, Prentice Hall international series in the physical and chemical engineering sciences. Prentice Hall, Boston.

Tables

Table S1. Stream data for energy targeting

Stream number	Stream name	Supply temperature (°C)	Target temperature (°C)	Duty (kW)	Stream type
1	Feed heating	35	126	406	Cold
2	Reboiler esterification	182	183	427	Cold
3	Condenser hydrolysis	59	58	-889	Hot
4	Reboiler hydrolysis	106	107	448	Cold
5	Condenser recovery	66	65	-246	Hot
6	Reboiler recovery	98	99	267	Cold
7	Vapour from flash	105	100	-311	Hot

Table S2. Utilities included in the energy targeting analysis **(Turton, 2018)**

Utility	Supply temperature (°C)	Target temperature (°C)	Cost ($/kW h)
Cooling water	25	30	0.0013608
LP steam	160	159	0.016344
HP steam	250	249	0.020376

Table S3. Boiling temperatures of pure components and azeotropes at different pressures (the bold line represents the temperature limit set by the catalyst)

Component/ Azeotrope	Boiling points at different pressures								
	0.1 atm	0.2 atm	0.3 atm	0.4 atm	0.5 atm	0.6 atm	0.7 atm	1 atm	3 atm
MeOH	15.67	28.60	36.80	42.95	47.91	52.10	55.74	64.53	95.36
Water-DMS	45.65	59.77	68.72	75.41	80.82	85.37	89.33	98.89	132.34
ML-Water	46.01	60.22	69.22	75.96	81.40	85.99	89.98	99.62	133.46
Water	46.06	60.35	69.41	76.19	81.67	86.29	90.31	100.02	134.05
ML	81.92	98.35	108.85	116.75	123.16	128.59	133.32	144.81	185.8
LA-DMS	125.14	143.11	154.5	163	169.86	175.64	180.66	192.75	234.55
(Di-LA)-DMS	124.89	142.91	154.41	189.3	170.06	175.98	181.13	193.61	237.43
DMS-MMS	-	-	-	-	-	-	-	-	243.62
DMS	125.24	143.61	155.43	164.36	171.63	177.81	183.21	196.37	243.63
Di-LA	150.64	167.88	178.83	187.03	193.65	199.25	204.11	215.88	257.25
LA-MMS	154.59	171.12	181.53	189.3	195.54	200.78	205.33	216.35	-
LA	156.52	172.46	182.56	190.12	196.22	201.36	205.84	216.63	254.32
MMS	165.14	173.66	184.83	193.21	200	205.75	210.75	222.88	265.82
SA	244.53	263.67	275.87	285.04	292.47	298.77	304.26	317.6	365.41
Tri-LA	272.25	291.8	304.2	313.46	320.94	327.24	332.71	345.9	391.55
Number of azeotropes	5	5	5	5	5	5	5	6	5

Table S4. Initialisation values from the shortcut calculations for a liquid split ratio of 0.4

Mole flowrate (kmol/h)	LA solution	MeOH feed	Impu-rities	Vapour to hydrolysis	Returning stream	Liquid to hydrolysis	Vapour from hydrolysis	Excess MeOH and water	Concentrated LA
MeOH	-	5.202	-	-	-	-	4.140	4.140	-
Water	14.598	0.053	-	24.495	4.642	6.963	-	12.889	-
ML	-	-	-	6.900	2.760	4.140	-	-	-
DMS	-	-	0.531	-	-	-	-	-	-
LA	4.140	-	-	-	-	-	-	-	4.140
SA	0.531	-	-	-	-	-	-	-	-

Table S5. Setup parameters and results of the sensitivity analysis over the liquid split ratio

Test	Units	Test 1	Test 2	Test 3	Test 4	Test 5
Setup parameters						
Vary variable Liquid split ratio		**0.1**	**0.2**	**0.3**	**0.4**	**0.5**
Pressure	atm	0.5	0.5	0.5	0.5	0.5
B/F		0.021	0.019	0.018	0.017	0.015
Type of condenser		none	none	none	none	none
Mass holdup per stage	kg	10	10	10	10	10
Temperature constraint for reactive zone (stage 24)	°C	145	145	145	145	145
Total stages		29	29	29	29	29
Rectifying stages		4 (1-4)	4 (1-4)	4 (1-4)	4 (1-4)	4 (1-4)
Reactive stages		20 (5-24)	20 (5-24)	20 (5-24)	20 (5-24)	20 (5-24)
Stripping stages		5 (25-29)	5 (25-29)	5 (25-29)	5 (25-29)	5 (25-29)
Feed stage for LA		3	3	3	3	3
Feed stage for MeOH		24	24	24	24	24
Returning stream flowrate	kmol/h	1.23	2.78	4.76	7.40	11.10
ML	mol fr	0.37	0.37	0.37	0.37	0.37
Water	mol fr	0.63	0.63	0.63	0.63	0.63
Temperature returning stream	°C	84	84	84	84	84
Key results tracked						
MeOH feed flowrate makeup with a design spec in the last reactive stage	kmol/h	3.57	6.07	4.432	4.72	5.16
B/F recalculated after MeOH makeup adjustment		0.018	0.016	0.017	0.017	0.017
Top temperature	°C	87.1	86.6	88.4	89.4	90.5
Bottom temperature	°C	180.3	176.6	182.3	185.4	187.9
Reboiler duty	kW	311.1	354.5	357.9	389.1	433.2
LA conversion	%	99.54	99.96	99.40	98.94	98.99
Di-LA&Tri-LA bottom	mol fr	0.075	0.031	0.055	0.050	0.039
Impurities bottom	mol fr	0.893	0.966	0.903	0.877	0.890

Table S6. Flowsheet stream table

Stream number	**1**	**2**	**3**	**4**	**5**	**6**	**7**	**8**	**9**	**10**	**11**	**12**	**13**
Temperature (°C)	35.0	126.0	105.4	105.4	105.4	30.0	183.1	83.0	78.2	106.9	57.6	99.2	64.7
Pressure (atm)	2.0	2.0	1.0	1.0	1.0	2.0	0.5	0.5	0.5	0.5	1.0	1.0	1.0
Vapour fraction	0.00	0.51	0.55	0.00	1.00	0.00	0.00	1.00	0.00	0.00	0.00	0.00	0.00
Mass flow (kg/h)	1255.2	1255.2	1255.2	760.5	494.7	26.1	73.3	1200.9	79.0	411.3	710.6	301.9	408.7
Mole flow (kmol/h)	50.00	50.00	50.00	22.65	27.35	0.81	0.54	38.51	2.78	6.62	29.12	16.30	12.81
Component mole flowrates (kmol/h)													
Lactic acid	4.181	4.181	4.181	4.152	0.029	0.000	0.005	0.001	0.080	4.001	0.000	0.000	0.000
Dilactic acid	0.000	0.000	0.000	0.000	0.000	0.000	0.008	0.000	0.000	0.009	0.000	0.000	0.000
Trilactic acid	0.000	0.000	0.000	0.000	0.000	0.000	0.000	0.000	0.000	0.000	0.000	0.000	0.000
Methyl lactate	0.000	0.000	0.000	0.000	0.000	0.000	0.000	4.459	0.250	0.028	0.082	0.082	0.000
Methanol	0.000	0.000	0.000	0.000	0.000	0.813	0.000	8.778	0.119	0.000	12.758	0.075	12.683
Water	45.288	45.288	45.288	17.971	27.317	0.000	0.000	25.276	2.332	2.579	16.275	16.147	0.128
Succinic acid	0.531	0.531	0.531	0.531	0.000	0.000	0.128	0.000	0.000	0.000	0.000	0.000	0.000
DMS	0.000	0.000	0.000	0.000	0.000	0.000	0.224	0.000	0.000	0.000	0.000	0.000	0.000
MMS	0.000	0.000	0.000	0.000	0.000	0.000	0.179	0.000	0.000	0.000	0.000	0.000	0.000
Component mole fraction													
Lactic acid	0.084	0.084	0.084	0.183	0.001	0.000	0.009	0.000	0.029	0.605	0.000	0.000	0.000
Dilactic acid	0.000	0.000	0.000	0.000	0.000	0.000	0.016	0.000	0.000	0.001	0.000	0.000	0.000
Trilactic acid	0.000	0.000	0.000	0.000	0.000	0.000	0.000	0.000	0.000	0.000	0.000	0.000	0.000
Methyl lactate	0.000	0.000	0.000	0.000	0.000	0.000	0.000	0.116	0.090	0.004	0.003	0.005	0.000
Methanol	0.000	0.000	0.000	0.000	0.000	1.000	0.000	0.228	0.043	0.000	0.438	0.005	0.990
Water	0.906	0.906	0.906	0.793	0.999	0.000	0.000	0.656	0.839	0.390	0.559	0.990	0.010
Succinic acid	0.011	0.011	0.011	0.023	0.000	0.000	0.234	0.000	0.000	0.000	0.000	0.000	0.000
DMS	0.000	0.000	0.000	0.000	0.000	0.000	0.412	0.000	0.000	0.000	0.000	0.000	0.000
MMS	0.000	0.000	0.000	0.000	0.000	0.000	0.330	0.000	0.000	0.000	0.000	0.000	0.000

Table S7. Flowsheet design results

Parameter	**C-1**	**C-2**	**C-3**
Pressure (atm)	0.5	0.5	1
Total number of trays	25	85	30
Number of rectifying stages	8	10	15
Number of reactive stages	12	30	-
Number of stripping stages	5	45	15
Catalyst mass per stage (kg)	10.0	12.0 (11-40) 14.0 (41-80)	-
Maximum stage liquid holdup (m^3)	0.00478*	0.00262*	0.00129
Feed stage	6 (LA) 20 (MeOH)	21	16
Condenser duty (kW)	0	889	246
Reboiler duty (kW)	427	448	267
Diameter (m)	0.67	0.57	0.33

* The liquid stage holdup corresponds to 3 % of the total stage volume with a HETP of 0.4 m, assuming a catalyst occupancy of 50 % of the holdup volume and a catalyst bulk density of 800 kg/m^3

Figures

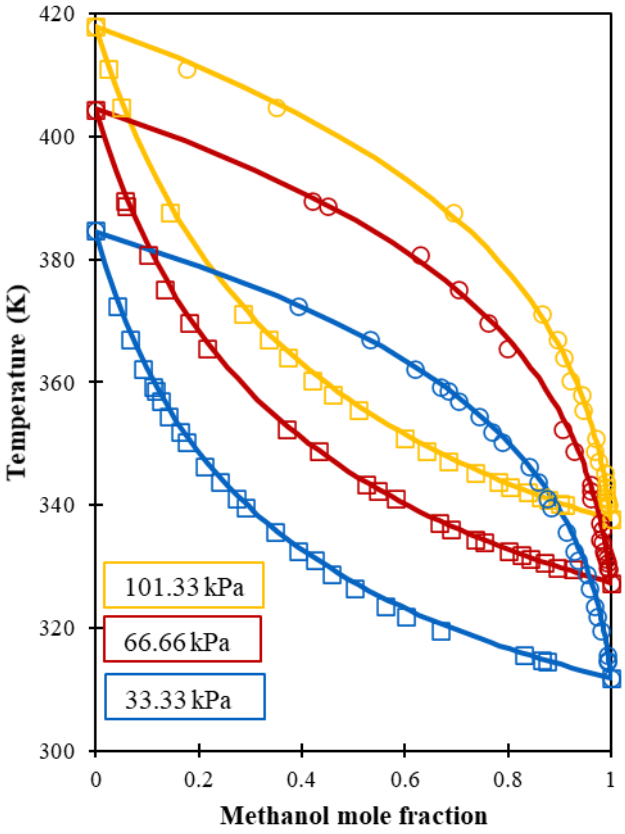

Figure S1. VLE validation for the methyl lactate-methanol system at different pressures (solid line: predicted values, □ : experimental mole fraction in the liquid phase, ○ : experimental mole fraction in the vapour phase)

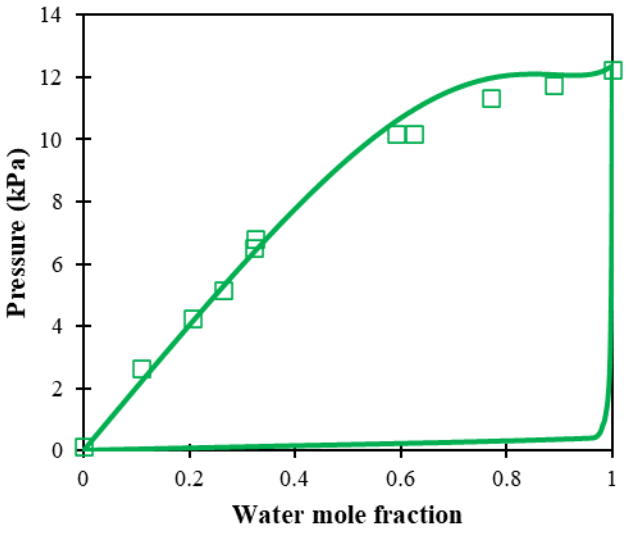

Figure S2. VLE validation for the monomethyl succinate-water system at 323.15 K (solid line: predicted values, □ : experimental mole fraction of water in the liquid phase)

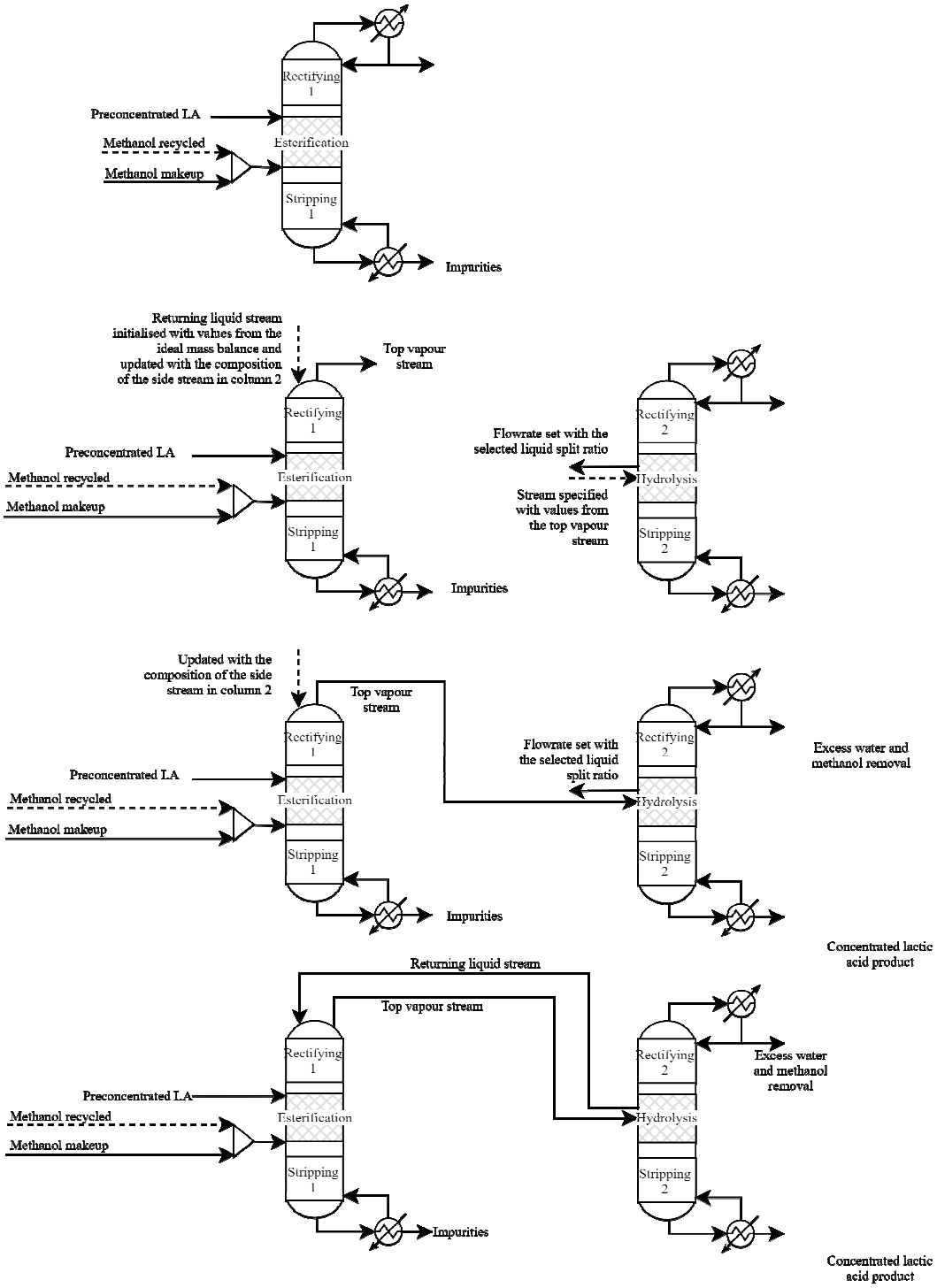

Figure S3. Coupling procedure for the simulation of the dual R-DWC in Aspen Plus

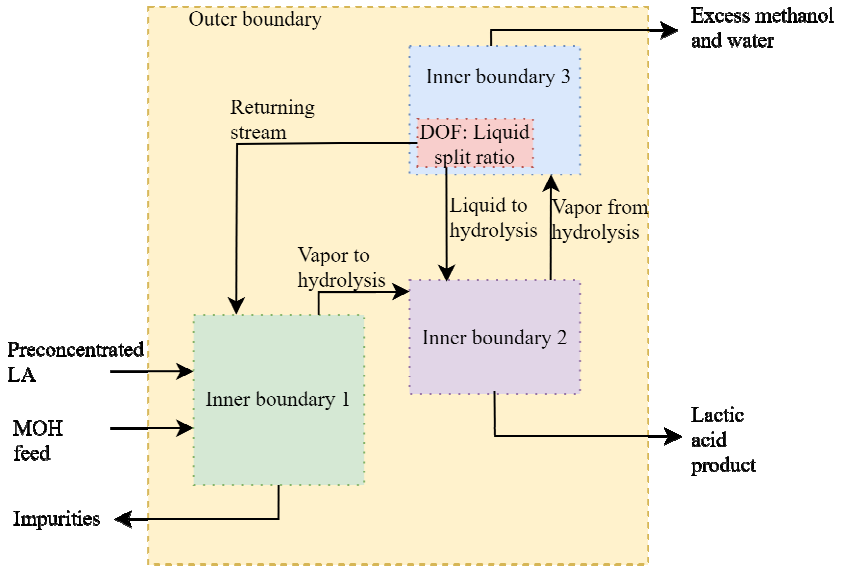

Figure S4. Block diagram used for the shortcut calculations

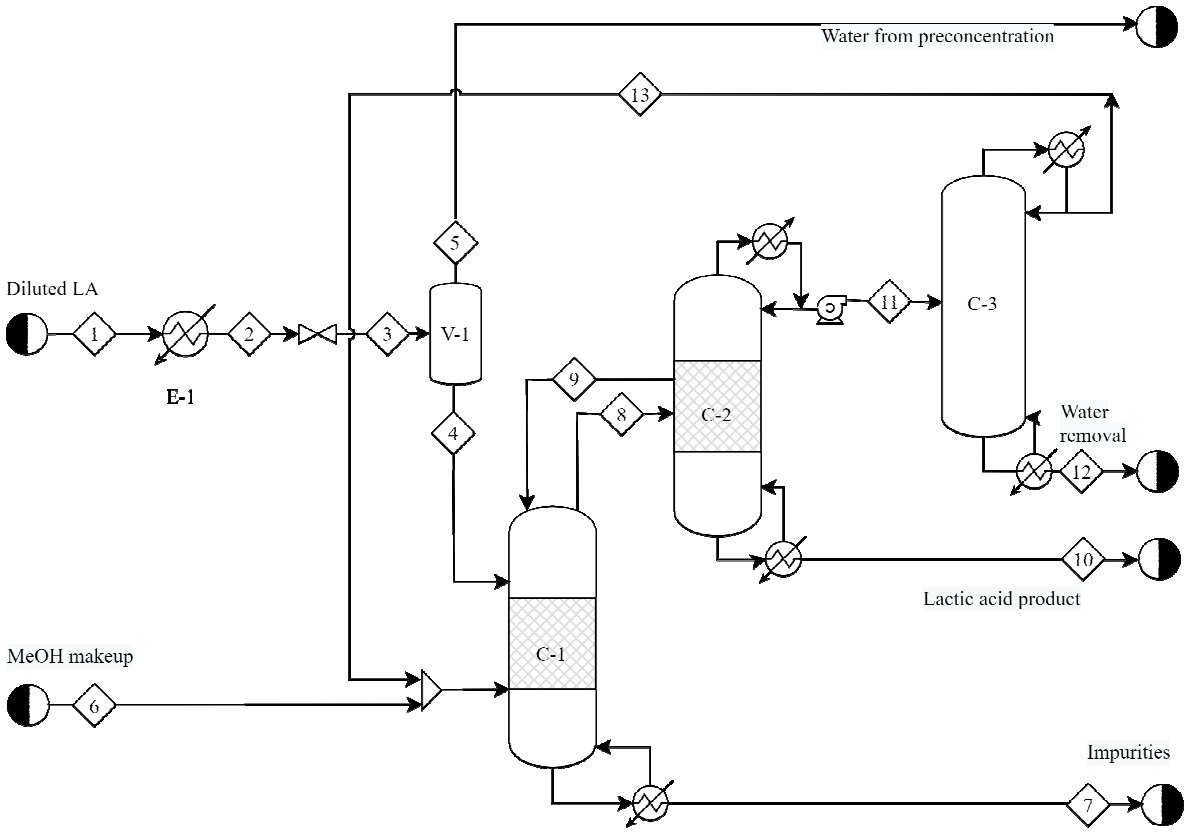

Figure S5. Process flowsheet developed for the preconcentration and purification of lactic acid